Structures of the dI_2dIII_1 Complex of Proton-Translocating Transhydrogenase with Bound, Inactive Analogues of NADH and NADPH Reveal Active Site Geometries[†,‡]

Tina Bhakta,[§] Simon J. Whitehead,[§] John S. Snaith,[||] Tim R. Dafforn,[§] John Wilkie,[||] Sundaresan Rajesh,[⊥] Scott A. White,[§] and J. Baz Jackson*[,§]

School of Biosciences, School of Chemistry, and Division of Cancer Studies, University of Birmingham, Edgbaston, Birmingham B15 2TT, U.K.

Received September 4, 2006; Revised Manuscript Received January 22, 2007

ABSTRACT: Transhydrogenase couples the redox reaction between NADH and $NADP^+$ to proton translocation across a membrane. The enzyme comprises three components; dI binds NAD(H), dIII binds NADP(H), and dII spans the membrane. The 1,4,5,6-tetrahydro analogue of NADH (designated H_2NADH) bound to isolated dI from *Rhodospirillum rubrum* transhydrogenase with similar affinity to the physiological nucleotide. Binding of either NADH or H_2NADH led to closure of the dI mobile loop. The 1,4,5,6-tetrahydro analogue of NADPH (H_2NADPH) bound very tightly to isolated *R. rubrum* dIII, but the rate constant for dissociation was greater than that for NADPH. The replacement of $NADP^+$ on dIII either with H_2NADPH or with NADPH caused a similar set of chemical shift alterations, signifying an equivalent conformational change. Despite similar binding properties to the natural nucleotides, neither H_2NADH nor H_2NADPH could serve as a hydride donor in transhydrogenation reactions. Mixtures of dI and dIII form dI_2dIII_1 complexes. The nucleotide charge distribution of complexes loaded either with H_2NADH and $NADP^+$ or with NAD^+ and H_2NADPH should more closely mimic the ground states for forward and reverse hydride transfer, respectively, than previously studied dead-end species. Crystal structures of such complexes at 2.6 and 2.3 Å resolution are described. A transition state for hydride transfer between dihydronicotinamide and nicotinamide derivatives determined in ab initio quantum mechanical calculations resembles the organization of nucleotides in the transhydrogenase active site in the crystal structure. Molecular dynamics simulations of the enzyme indicate that the (dihydro)nicotinamide rings remain close to a ground state for hydride transfer throughout a 1.4 ns trajectory.

Transhydrogenase is found in the cytoplasmic membrane of bacteria and in the inner membrane of mitochondria from animal cells. It couples the transfer of hydride ion equivalents between NAD(H)[1] and NADP(H) to the translocation of protons across the membrane.

$$NADH + NADP^+ + H^+_{out} \leftrightarrow NAD^+ + NADPH + H^+_{in} \quad (1)$$

Hydride transfer proceeds directly between bound nucleotides (*1*) and is stereospecific (*2*, *3*): the *pro-R* hydrogen at $C4_N$ of the dihydronicotinamide ring of NADH is transferred to $C4_N$ on the *si* face of the nicotinamide ring of $NADP^+$. In the "forward" direction, the enzyme is driven from left to right (eq 1) by the proton electrochemical gradient (Δp) generated by the respiratory (or sometimes photosynthetic) electron transport chain. One proton is translocated across the membrane through transhydrogenase per hydride ion transferred between nucleotides (*4*). There is broad agreement that conformational changes in the protein mediate coupling between the redox reaction and proton translocation (for reviews see refs *5*−*7*). Kinetic (*8*) and mutagenesis (*9*−*11*) experiments indicate that binding changes at the NADP(H)-binding site are central in this process. Transhydrogenase produces NADPH for biosynthesis reactions and for the

[†] This work was supported by the Biotechnology and Biological Sciences Research Council.

[‡] The two X-ray structures described in this paper are listed in the PDB as 2OOR (the dI_2dIII_1 complex with bound NAD^+ and 1,4,5,6-tetrahydronicotinamide adenine dinucleotide phosphate) and 2OO5 (the dI_2dIII_1 complex with bound 1,4,5,6-tetrahydronicotinamide adenine dinucleotide and $NADP^+$).

* To whom correspondence should be addressed: e-mail, j.b.jackson@bham.ac.uk; phone, +44 (0)121 414 5423; fax, +44 (0)121 414 5925.

[§] School of Biosciences, University of Birmingham.

[||] School of Chemistry, University of Birmingham.

[⊥] Division of Cancer Studies, University of Birmingham.

[1] Abbreviations: H_2NADH, 1,4,5,6-tetrahydronicotinamide adenine dinucleotide; H_2NADPH, 1,4,5,6-tetrahydronicotinamide adenine dinucleotide phosphate; $AcPdAD^+$, acetylpyridine adenine dinucleotide (oxidized form); Nic^+, nicotinamide; NicH, 1,4-dihydronicotinamide; H_2NicH, 1,4,5,6-tetrahydronicotinamide; NAD(H), NAD^+ or NADH etc.; $C4_N$, the carbon-4 atom of the nicotinamide (dihydronicotinamide etc.) ring; dI, the NAD(H)-binding component of transhydrogenase; dIII, the NADP(H)-binding component; dII, the membrane-spanning component; dIII.E155W, the dIII component whose Glu155 is replaced by a Trp residue.

10.1021/bi061843r CCC: $37.00
Published on Web 02/27/2007

reduction of glutathione needed to minimize free radical damage (*12*, *13*). Through a microcycle with the isocitrate dehydrogenases, it may participate in the control of the Krebs cycle in some cell types (*14*). Defects in the transhydrogenase gene lead to altered pathways of amino acid metabolism in *Escherichia coli* (*15*), to greater susceptibility to oxidative stress in *Rhodobacter sphaeroides* (*16*) and *Caenorhabditis elegans* (*17*), and to impaired control of glucose homeostasis in mice (*18*).

Two of the protein components of transhydrogenase, dI, which binds NAD(H), and dIII, which binds NADP(H), protrude from the membrane (on the cytoplasmic side in bacteria, the matrix side in mitochondria), and a third component, dII, spans the membrane [in 12−14 transmembrane helices, depending on species (*19*, *20*)]. The enzyme is probably a "dimer" of two dI-dII-dIII "monomers", though the polypeptide composition varies between species (see ref *21*). The crystal structure of intact transhydrogenase is unavailable, but structures of isolated recombinant dI (*22*−*24*) and dIII (*25*−*27*) have been solved for several species.

Mixtures of isolated dI and dIII from *Rhodospirillum rubrum* form a heterotrimeric dI_2dIII_1 complex, which can catalyze a single turnover of rapid hydride transfer between bound NAD(H) and NADP(H) or their analogues, even in the absence of the membrane-spanning dII (*1*, *28*−*31*). Crystal structures of the complex were obtained with bound NAD^+ and $NADP^+$ (*32*) and with bound NADH and NADPH (*33*). Having both nucleotides oxidized, or both reduced, prevents hydride transfer during crystallization. The structures of these "dead-end" complexes show that the hydride-transfer site is located at the dI/dIII interface. Of particular interest is the finding that the Nic(H) ring of the bound NAD(H) can occupy two positions, "distal" and "proximal" relative to the Nic(H) ring of the bound NADP(H). During the switch between the distal and proximal positions, the adenosine moiety of the NAD(H) remains fixed in its binding pocket, but rotations of bonds in the diphosphate and ribose phosphate region displace the Nic(H) ring. It was suggested that the positional switch of the Nic(H) ring of the NAD(H) may be important in gating the hydride-transfer reaction during proton translocation by the intact enzyme, and a plausible pathway linking the intermediate protein- and nucleotide-structural states involved in proton translocation was outlined (*5*). The asymmetries of the dI_2dIII_1 complex indicate that the two dI-dII-dIII monomers of intact transhydrogenase proceed through alternating, coupled, out-of-phase conformational changes during turnover (*21*, *32*).

In the ground state for hydride transfer, the active site will be occupied by NADH and $NADP^+$ during forward transhydrogenation (eq 1) and by NAD^+ and NADPH during reverse transhydrogenation. Because of their different charge balances, there is a possibility that the structures of NAD^+/$NADP^+$ and NADH/NADPH dead-end complexes might not accurately reflect the active site geometry in productive complexes. Recent attempts to crystallize dI_2dIII_1 with NADH (in excess) and $NADP^+$ have led either to dead-end NADH/NADPH complexes or to complexes with nucleotides having an unknown redox state (*34*). In another attempt to determine the structure of the hydride-transfer site and the important conformational changes that occur during the redox reaction, we now describe the results of experiments performed with 1,4,5,6-tetrahydro analogues of NADH and NADPH, in which the C5−C6 double bond of the dihydronicotinamide (NicH) ring of the physiological nucleotide has been reduced to a 1,4,5,6-tetrahydronicotinamide (H_2-NicH) ring (see Scheme 1). These nucleotide analogues (H_2NADH and H_2NADPH, respectively) have been shown to bind like NAD(P)H to a number of soluble dehydrogenases but to be blocked in their on-enzyme redox chemistry (*35*−*41*). Crystal structures of liver alcohol dehydrogenase (*40*) and malate dehydrogenase (*41*) with H_2NADH show binding interactions and conformational changes similar to those seen with the physiological nucleotide, indicating that the analogue provides a good model for the active site. Loading the transhydrogenase dI_2dIII_1 complex with combinations of analogue and physiological nucleotides enables us to reconstruct the active site of this proton-translocating enzyme with a charge balance that more closely resembles the ground states for hydride transfer than is found in dead-end complexes.

Scheme 1: Biological Oxidation of 1,4-Dihydronicotinamide (NicH) to Nicotinamide (Nic^+) and of 1,4,5,6-Tetrahydronicotinamide (H_2NicH) to 5,6-Dihydronicotinamide (H_2Nic^+)[a]

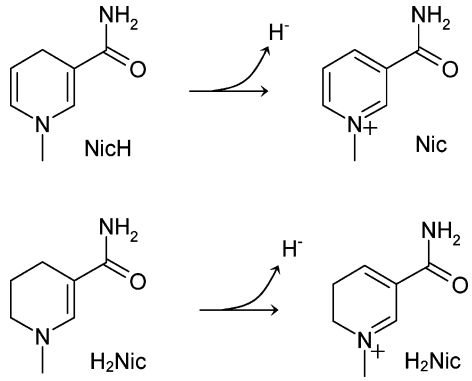

[a] NicH and Nic^+ represent the reduced and oxidized nicotinamide moieties of the physiological nucleotides, NAD(P)(H). H_2NicH and H_2Nic^+ represent the reduced and biologically oxidized (see text) moieties of the analogue nucleotides, H_2NAD(P)(H).

EXPERIMENTAL PROCEDURES

Cultures of *R. rubrum* were grown under phototrophic conditions in RCV medium (*42*) supplemented with either biotin (in the case of the wild-type strain, S1) or biotin *plus* tetracycline [in the case of the transhydrogenase-overexpressing strain, RTB2 (*4*)]. Intracytoplasmic membrane vesicles (chromatophores) were prepared by French press treatment of harvested cells (*43*) and resuspended in 10% sucrose (w/v) and 100 mM Tris-HCl, pH 8.0. The bacteriochlorophyll concentration was measured using the in vivo extinction coefficient given (*44*).

Wild-type dI and the wild-type and E155W mutant of dIII from *R. rubrum* transhydrogenase were expressed from plasmids pCD1 (*45*), pNIC2 (*46*), and pJDV1 (*47*), respectively, in *E. coli* strains C600 (for dI) and BL21(DE3) (for dIII), and then purified by column chromatography and stored at −20 °C, as described in the earlier reports. The proteins were routinely >95% pure as judged by SDS−PAGE. Their concentrations were determined by the microtannin assay (*48*); values are expressed as monomers unless otherwise stated.

H_2NADH and H_2NADPH were prepared by hydrogenation of NADH and NADPH, respectively, in water at pH 8.5 (NaOH) using a 10% Pd/C catalyst (Fluka), essentially as described (*35*, *49*). The reaction was terminated when 1.0 mol of hydrogen/mol of nucleotide was consumed. After removal of the catalyst by filtration through Celite, the H_2-NAD(P)H was purified by chromatography on Q-Sepharose Fast Flow (Amersham Biosciences) with a 4−400 mM gradient of NH_4HCO_3. The physiological nucleotides and the analogues were identified by their UV absorbance spectra (*49*). Purified fractions were lyophilized three times to remove NH_4HCO_3 and stored at −20 °C. The absorbance spectra of solutions used for experiments were checked before use (see ref *50*). Unlike NAD(P)H, neither H_2NADH nor H_2NADPH was significantly fluorescent.

"Reverse" transhydrogenation was measured as the reduction of AcPdAD$^+$, an analogue of NAD$^+$, by NADPH from the absorbance change at 375 nm [$\epsilon = 6.1$ mM^{-1} cm^{-1} (*51*)]. Measurements in the steady state were performed on a Shimadzu UV2401 and in the transient state after rapid mixing on a DX-17MV Applied Photophysics stopped-flow spectrophotometer. As normally prepared, isolated dIII is associated with tightly bound NADP$^+$. For stopped-flow experiments, stored dIII (40 μM) was dialyzed overnight at 4 °C against 10 mM $(NH_4)_2SO_4$ and 20 mM Hepes, pH 8.0 ("SF buffer"). The protein was then concentrated to about 800 μM using a Vivaspin 20 kDa filter. A sample of this solution was mixed with H_2NADPH in SF buffer to give 100 μM dIII and 200 μM nucleotide, and this was incubated on ice for 2 h. An equal volume of a 200 μM solution of dI in SF buffer was added, and the mixture was loaded into one drive syringe of the stopped-flow machine; the other drive syringe contained 2.0 mM AcPdAD$^+$ in SF buffer. Parallel experiments were performed as a control using NADPH instead of H_2NADPH. The stopped-flow machine was operated with 1:1 mixing at 20 °C; the dead time was 1.31 ms (*1*).

Fluorescence changes were recorded on a Spex Fluoromax. Isothermal titration calorimetry on isolated dI was initially carried out at 20 °C using the MicroCal MCS system, as described (*52*), but further experiments, including those with the dI_2dIII_1 complex, were performed (with guidance from Margaret Nutley and Alan Cooper at the University of Glasgow) on a MicroCal VP to improve resolution. One-dimensional ^{1}H NMR experiments on dI were performed using a Brucker AMX 500 MHz spectrometer equipped with an HCN 5 mm Z-PFG cryoprobe essentially as described (*53*). The protein for these experiments was washed in 10 mM [^{2}H]Tris-HCl, pH 7.6, 1.0 mM dithiothreitol, 10 mM $(NH_4)_2SO_4$, and 0.025% NaN_3 in ^2H_2O and concentrated to 405 μM in the same buffer by centrifugation through Vivaspin 10 kDa filters before being loaded into the NMR tube. Heteronuclear spin quantum coherence (HSQC) spectra of 200 μM ^{15}N-labeled dIII protein in its NADP$^+$ form, prepared as described (*54*), were recorded at 30 °C on a Varian Inova 800 MHz spectrometer equipped with a room temperature 5 mm ^{1}H/^{13}C/^{15}N Z-PFG probe. The bound NADP$^+$ was then exchanged for either NADPH or H_2-NADPH, also as described (*54*), and HSQC spectra were recorded again. The data were processed using the AZARA 2.7 software suite (Boucher, http://www.bio.cam.ac.uk/azara/) and analyzed and visualized with the OpenGL version of ANSIG (*55*). The combined chemical shift changes (Δ_δ) in backbone ^{1}H and ^{15}N atoms upon nucleotide replacement were calculated as described (*56*).

Table 1: X-ray Data Collection and Refinement Statistics

	dI_2dIII_1	
	H_2NADH·NADP$^+$	NAD$^+$·H_2NADPH
data collection statistics[a]		
unit cell parameters		
a, *b*, *c* (Å)	71.2, 101.0, 131.7	72.2, 74.4, 204.8
α, β, γ (deg)	90, 90, 90	90, 90, 90
resolution (Å)	62.6−2.6 (2.74−2.60)	68.0−2.32 (2.45−2.32)
completeness (%)	92.8 (94.4)	91.4 (69)
multiplicity	3.8 (3.1)	4.2 (3.6)
$I/\sigma I$	15.1 (4.0)	16.5 (3.4)
no. of observations	103525 (12512)	184225 (17038)
no. of unique observations	27548 (4046)	44362 (4726)
R_{sym}[b]	7.3 (22.7)	5.3 (31.7)
refinement statistics		
Wilson *B*/average *B*[c]	49.9/40.7	47.4/57.5
no. of non-hydrogen atoms/waters	7084/27	6984/101
rmsd[d] bond (Å)/ angle (deg)	0.008/1.252	0.009/1.337
Ramachandran[e] (%)	91.5, 8.3, 0.1, 0.1	91.6, 7.9, 0.5, 0.0
R/R_{free}	21.9/27.5	24.7/27.5
PDB code	2OO5	2OOR

[a] Numbers in parentheses indicate data for the highest resolution shell. [b] $R_{sym} = \sum_j|\langle I\rangle - I_j|/\sum\langle I\rangle$, where I_j is the intensity of the *j*th reflection and $\langle I\rangle$ is the average intensity. [c] As calculated for all atoms. [d] rmsd is the root mean square deviation from ideal values. [e] The percentage of residues in the core, allowed, generously allowed, and disallowed regions, respectively, as measured by the program PROCHECK.

The dI and dIII proteins were prepared for crystallography by dialysis against 10 mM Hepes, pH 8.0, and then spin concentrated (see above). The dI_2dIII_1 complex in its H_2-NADH/NADP$^+$ form was crystallized from equimolar solutions of dI and dIII containing 5 mM H_2NADH and 5 mM NADP$^+$ in 100 mM Tris-HCl, pH 8.0, 75 mM Li_2SO_4, 16−20% 4K polyethylene glycol, and 10% glycerol. Before the dI_2dIII_1 complex was crystallized in its NAD$^+$/H_2NADPH form, NADP$^+$ on the dIII protein was exchanged by incubating the protein solution (300 μM) with 5 mM H_2-NADPH for 2 h. Crystals were then grown from equimolar solutions of dI and dIII containing 50 mM NAD$^+$ and 5 mM H_2NADPH in 25−70 mM ammonium sulfate, 100 mM Mes, pH 6.5, 15−18% 4K polyethylene glycol, and 10% glycerol. Complete data sets of the H_2NADH/NADP$^+$ crystals were collected to 2.6 Å on beamline ID14-4 at the European Synchrotron Radiation Facility at Grenoble, France, and of the NAD$^+$/H_2NADPH crystals to 2.3 Å on beamline ID14-3. The data were integrated and scaled using the programs MOSFLM (*57*) and SCALA (*58*). The H_2NADH/NADP$^+$ crystal had different cell dimensions (Table 1) to those previously reported for the NADH/NADPH crystal (PDB code 1U2D), and therefore, molecular replacement was used to determine the initial phases. The 1U2D structure was used as a search model against the data (up to 4 Å) for the H_2-NADH/NADP$^+$ crystal in the program EPMR (*59*). The solution from molecular replacement was subjected to rigid body refinement in REFMAC5 (*60*). Simulated annealing protocols were also applied using the program CNS (*61*). The NAD$^+$/H_2NADPH crystal was isomorphous with the

$NAD^+/NADP^+$ structure (PDB code 1HZZ), which was subsequently used to refine against the structure factor amplitudes of the NAD^+/H_2NADPH crystal using REFMAC5. Simulated annealing protocols were applied using CNS before the model was adjusted to accommodate the new nucleotide combination. The two new structures were further subjected to constrained refinement with TLS in REFMAC5. The final models were assessed and adjusted according to the programs Whatcheck (*62*) and Procheck (*63*). Superposition of crystal structures was performed using LSQKAB from the CCP4 program suite, and domain rotations in dI were analyzed with the MORPH server (*64*) (Figure 8).

The molecular dynamics (MD) study was performed on the crystal structure of the dI_2dIII_1 complex (PDB code 2OO5) using AMBER 8 (*65*). Atomic partial charges for the nicotinamide nucleotides were determined using the method (*66*). The atom-centered charges on the Nic^+ and H_2NicH rings, and the diphosphate and 2′-phosphate groups, were derived in two stages coordinated by RED II (www.u-picardie.fr/labo/lbpd/RED). First, GAUSSIAN 98 (*67*), using the HF/6-31G* basis set, performed an ab initio structural optimization to calculate a three-dimensional molecular electrostatic potential. Then, in accordance with the RESP method (*68*), a two-stage fitting procedure was performed (RESP from AMBER 8) to calculate a model of atom-centered partial charges. The atom-centered charges of the adenine and ribose moieties were obtained from the RA3 R-adenosine unit in the AMBER ff94 force field (*69*). The structural parameters for the nicotinamide nucleotides were provided by the general AMBER force field (gaff) (*70*). The amino acids were described using the AMBER ff03 force field (*71*). The protein was stripped of crystallographic waters and then solvated with 32813 TIP3P waters (*72*). The solvent coordinates were then minimized, and the water positions were randomized by a short MD simulation of 20 ps at 300 K. Following this, the entire system (112709 atoms) was minimized and subjected to a 250 ps equilibration at 300 K. A time step of 2 fs was employed throughout, and atomic velocities were scaled using the Berendsen algorithm (*73*) to maintain the system temperature at 300 K. MD simulations were performed for 1 ns using the NVT ensemble, and coordinates were saved every 0.5 ps. Bonds between hydrogens and heavy atoms were constrained using the SHAKE algorithm (*74*), long-range electrostatics were calculated using the particle-mesh Ewald method (*75*), and nonbonding interactions were cut off at an 8 Å radius. All calculations were performed on the escience cluster at the University of Birmingham. Structures along the MD trajectory were manipulated, ring centers were defined, and ring tilts were determined, using GEOMALC from the CCP4 suite of programs.

Transition states for hydride transfer were determined using density function theory with GAUSSIAN98. A combination of Baronne's 1-parameter modified Perdew-Wang 91 exchange functional and the Perdew-Wang 91 correlation functional (MPW1PW91) was used along with a 6-31G** basis set. Transition states were characterized by means of frequency calculations to confirm that they were genuine first-order transition states and that the transition vector corresponded to the hydride transfer reaction. *N*-Methylnicotinamide was used as a model for both NADP(H) and NAD(H). Starting structures were generated from initial transition state calculations for hydride transfer between dihydropyridine and protonated pyridinium cation following the approach of Wu et al. (*76*). Amide groups were added at appropriate positions to a C_2 symmetrical structure (with dihydropyridine rings rotated by 120° around a C_4-C_4 axis, thus corresponding to the arrangement seen in the crystal structure) and a C_{2v} structure previously indicated to give the lowest energy transition state (*76*). The C_{2h} structure of Wu et al. (*76*) was not considered as this previous work had indicated that it led to transition states of considerably higher energy. Thus, starting points were generated for all possible combinations of amide position and orientation on a C_2 symmetrical core in addition to those corresponding to the "cis" and "trans" structures of Wu et al. (*76*). It should be noted, however, that the calculations described here are at a higher level of theory and involve a model modified from that of Wu et al. The results therefore are not strictly comparable (*76*). A further difference is that we have considered arrangements of amide bonds that generate asymmetric transition states.

The structure cartoons (Figures 3, 4, 7, and 8) were constructed using the program PYMOL (*77*) and the diagrams in Figure 5f,g using SWISS-PDV VIEWER. Amino acid residues are numbered according to the convention adopted (*32*).

RESULTS

Binding of H_2NADH to the dI Component of Transhydrogenase. To assess whether H_2NADH and H_2NADPH are good analogues of NADH and NADPH, respectively, their binding to the recombinant dI and dIII components of *R. rubrum* transhydrogenase was investigated. *R. rubrum* dI has a single Trp residue (at position 72) whose fluorescence emission is quenched upon addition of NADH but not NADPH (*45*). Addition of H_2NADH to a solution of isolated dI also led to the quenching of Trp72 fluorescence. K_d values calculated from titrations, after appropriate corrections for inner filtering effects, were similar: 18 μM for NADH (*45*) and 27 μM for H_2NADH (see Figure S1, Supporting Information). The binding of H_2NAD to isolated dI was also studied by isothermal titration calorimetry. The experiments revealed binding characteristics very similar to those of NADH (*52*). The K_d for H_2NADH was 24 μM [18 μM for NADH (*52*)], the enthalpy change was -45 kJ mol^{-1} dI monomer (-62 kJ mol^{-1} monomer for NADH), and for both the analogue and the natural nucleotide, the binding stoichiometry was approximately 1 per dI monomer (see Figure S2, Supporting Information).

In one-dimensional proton NMR experiments, the addition of NADH to isolated dI leads to line broadening and to changes in the chemical shift of relatively narrow resonances arising from a "mobile loop" (residues 220−240) in the protein (*53*, *78*). The effects are attributable to a loss in mobility of residues in the loop as it closes down on the protein surface during nucleotide binding. The addition of H_2NADH to a solution of dI had very similar effects on the NMR spectrum: the same set of resonances was affected (see ref *78* for partial assignments) and in an equivalent way (Figure S3, Supporting Information). This indicates that the physiological and analogue nucleotides cause a similar conformational change in dI upon binding. The concentration

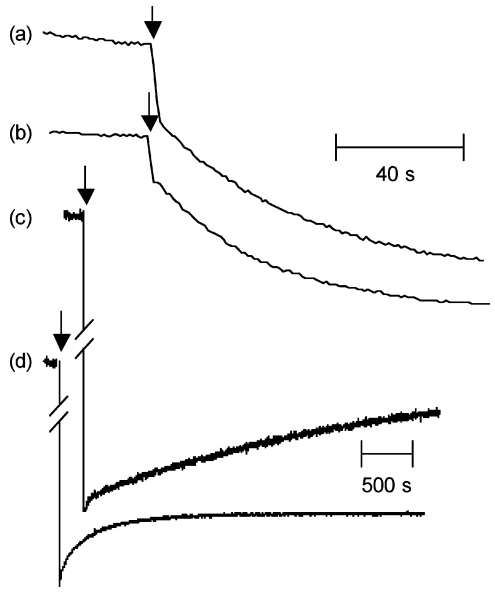

FIGURE 1: Changes in the fluorescence of Trp155 as dIII.E155W undergoes nucleotide exchange. (a) The fluorescence emission at 338 nm from excitation at 280 nm (4 nm band-pass) was recorded during addition of 10 μM NADPH (arrow) to a solution of the $NADP^+$ form of dIII.E155W (1.0 μM) in 20 mM MOPS, pH 7.2 at 25 °C. (b) The fluorescence emission was recorded during addition of 10 μM H_2NADPH to another sample of the same protein under similar conditions. (c) The $NADP^+$ on dIIII.E155W was first exchanged with NADPH as described in the text, and the 338−280 nm fluorescence change was then recorded during addition of 500 μM $NADP^+$ to a 1.0 μM solution of this protein in the conditions stated above. The large, initial inner-filtering effect of the nucleotide has been partially removed from the trace where indicated. (d) As in (c) except that the $NADP^+$ on dIIII.E155W was first exchanged with H_2NADPH.

dependences were similar for NADH and for H_2NADH, but because the nucleotides are in intermediate exchange with the protein, the broadened resonances make the end points of the titrations difficult to judge accurately. Nevertheless, the data are consistent with K_d values in the order of 20 μM for both NADH and H_2NADH.

It should be noted that NAD^+ binds much more weakly to dI than either NADH or H_2NADH. The K_d for NAD^+ is approximately 300 μM (*79*, *80*).

Binding of H_2NADPH to the dIII Component of Transhydrogenase. The isolated dIII component of *R. rubrum* transhydrogenase binds NADP(H) very tightly (*28*). The K_d values are too low to measure. To compare the binding of H_2NADPH with that of NADPH, we have performed experiments to measure rates of nucleotide exchange from dIII. In dIII.E155W, a unique Trp residue replaces the wild-type Glu155. The catalytic properties of the mutant protein are similar to those of wild-type dIII, but the fluorescence emission from the Trp usefully reflects nucleotide occupation (*47*) (and see ref *81*). Thus, the Trp fluorescence is greater when $NADP^+$ is bound to the protein than when NADPH is bound. In the experiments shown in panels a and b of Figure 1, NADPH and H_2NADPH, respectively, were added to solutions containing dIII in its $NADP^+$ form. Following the rapid initial decrease due to the inner-filtering effect of the added nucleotide, the Trp155 fluorescence slowly declined over a period of >100 s with approximately similar kinetics. According to earlier reasoning (*47*, *81*), the results suggest that slow dissociation of bound $NADP^+$ from dIII ($k_{off} \approx$ 0.03 s^{-1}) is followed by the rebinding of either NADPH or H_2NADPH. Evidently, H_2NADPH can bind to dIII and quench Trp fluorescence in a similar way to the natural nucleotide.

In another set of experiments dIII.E155W was preincubated with either NADPH (Figure 1c) or H_2NADPH (Figure 1d) to load the protein with the respective nucleotide. A relatively high concentration of $NADP^+$ was then added to each of the two protein samples. Following the prompt fluorescence decrease due to inner-filtering effects, there was a very slow increase in fluorescence in both experiments that is attributable to nucleotide exchange. The very slow rate of exchange is consistent with the tight binding of NADPH and H_2NADPH to dIII (i.e., slow rates of dissociation). When the concentration of added $NADP^+$ is high enough, the exchange becomes limited by the dissociation of NADPH/H_2NADPH from the protein, and therefore, in the limit, the rate constant for the fluorescence increase corresponds to that for NADPH/H_2NADPH release. The dissociation rate constant for dIII.NADPH estimated from Figure 1c is similar to that described in an earlier report ($\approx 4 \times 10^{-4}$ s^{-1}), but that for dIII.H_2NADPH (though still small in absolute terms) is significantly greater than for the physiological nucleotide, about 3×10^{-3} s^{-1} (Figure 1d).

In the HSQC experiment the spins of ^1H and ^{15}N atoms in amide groups (both side chain and backbone) are correlated. The HSQC spectrum of isolated dIII from *R. rubrum* transhydrogenase in its $NADP^+$-bound form is almost fully assigned (*27*). When the bound $NADP^+$ is replaced by NADPH, there are chemical shift changes in distinctive subsets of the spectral peaks (*54*). Some of these chemical shift changes derive from amide groups of amino acid residues either close to or in contact with the NADP(H), but of particular interest are sensitive residues which extend some distance from the bound nucleotide into helix A, helix B, helix D/loop D, and loop E. The results indicate that there are changes in the magnetic environment within these regions, conformational changes in the protein, when the bound nucleotide becomes reduced. Similar data have been reported for isolated *E. coli* dIII (*82*). Figure 2 (top panel) shows the chemical shift changes in the HSQC spectrum of *R. rubrum* dIII when bound $NADP^+$ was replaced by H_2-NADPH. The changes are in the same regions of the polypeptide as those affected when bound $NADP^+$ is replaced by NADPH, indicating that the two reduced nucleotides have analogous effects on the dIII structure. However, Figure 2 (lower panel) reveals a difference in the extent of the chemical shift changes caused by NADPH and H_2NADPH. Relative to the chemical shift changes induced by replacing $NADP^+$ by NADPH, those induced by replacing $NADP^+$ by H_2NADPH are less pronounced in helix D/loop D (residues 135−146) than in helices A and B and loop E. Thus, the character of the conformational change caused by the nucleotide substitution seems to be subtly different for H_2NADPH and for NADPH in helix D/loop D. Conformational changes are not observed in dIII crystal structures when $NADP^+$ is replaced by NADPH (*33*, *83*), and therefore, those detected by NMR may correspond only to small atomic displacements. However, in one set of crystallization conditions a conformational rearrangement is evident in the helix D/loop D region but is similar when either $NADP^+$ or NADPH is bound (*83*). Changes in the redox state of bound

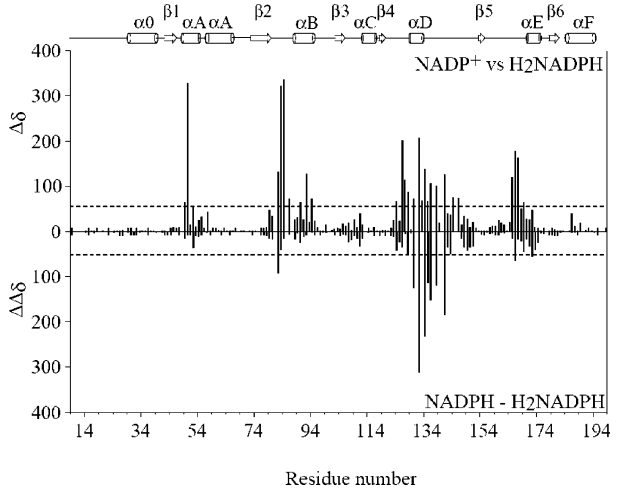

FIGURE 2: Chemical shift changes in dIII caused by substitution of bound $NADP^+$ with H_2NADPH and with NADPH. Upper panel: The HSQC spectrum of ^{15}N-labeled dIII in its $NADP^+$ form was recorded as described in the Experimental Procedures. Excess H_2NADPH was then added to the sample, and the spectrum was rerecorded (compare ref *54*). The change in chemical shifts of backbone amides between the two spectra, Δ_δ, is plotted as a function of residue number. Lower panel: An equivalent experiment was performed but using NADPH instead of H_2NADPH (as in ref *54*). The $\Delta\Delta_\delta$ values (i.e., the difference between Δ_δ from the $NADP^+$ *minus* H_2NADPH spectra and Δ_δ from the $NADP^+$ *minus* NADPH spectra) are plotted for each residue. The dashed lines correspond to twice the mean perturbation value (50 Hz) and indicate a significant change. The secondary structure of dIII is represented at the top of the figure.

NADP(H) are required to signal a reset in the proton translocation gate of dII (*8*), and the signal transmission pathway between dIII and dII might involve helix D/loop D (*5*). The small difference in structure between NADPH and H_2NADPH that is sensed by the chemical shift changes may be a reflection of this event.

H_2NADH and H_2NADPH Are Not Hydride Donors in the Transhydrogenase Reaction. Forward transhydrogenation (see eq 1) is conveniently measured by following the reduction of thio-$NADP^+$ (an analogue of $NADP^+$) with NADH. As in earlier experiments (*84*), the rate of this reaction was low in a sample suspension of darkened chromatophore membranes from *R. rubrum* strain RTB2 [0.29 μmol of thio-$NADP^+$ reduced (μmol of bacteriochlorophyll)$^{-1}$ min^{-1}] but was accelerated about 6-fold upon illumination with near-infrared light. Stimulation results from the generation of Δp by the photosynthetic electron transport chain: the increased Δp drives H^+ back across the membrane through the transhydrogenase. In contrast to NADH, H_2-NADH was unable to reduce thio-$NADP^+$ at a measurable rate in either darkened or illuminated chromatophore suspensions.

Reverse transhydrogenation can be monitored by following the reduction of $AcPdAD^+$ (an NAD^+ analogue) by NADPH (*51*). Wild-type chromatophore membranes catalyzed a rapid rate of this reaction [2.7 μmol of $AcPdAD^+$ reduced (μmol of bacteriochlorophyll)$^{-1}$ min^{-1}] but failed to catalyze $AcPdAD^+$ reduction with H_2NADPH. In a separate series of experiments (Figure S4, Supporting Information), it was found that the reduction of $AcPdAD^+$ by NADPH was inhibited by H_2NADH and by H_2NADPH, consistent with a competitive interaction at the respective binding sites.

Mixtures of purified dI and dIII from *R. rubrum* transhydrogenase spontaneously form a dI_2dIII_1 complex which catalyzes a rapid, single turnover burst of hydride transfer (*1*, *28*, *52*). Further turnovers are heavily limited by the very slow rate of release of product NADP(H) from the dIII component of the complex. The kinetics of the hydride-transfer burst in dI_2dIII_1 complexes can be observed in stopped-flow experiments using NADPH and $AcPdAD^+$ as substrates; the apparent first-order rate constant (k_{app}) is $\approx$600 s^{-1} (*30*). However, under conditions similar to those described earlier there was no detectable $AcPdAD^+$ reduction when NADPH was replaced by H_2NADPH. Within the experimental constraints k_{app} for this reaction is <3 s^{-1} (data not shown).

The dI_2dIII_1 complex catalyzes a rapid, steady-state "cyclic transhydrogenation" reaction in which tightly bound NADP(H) is alternately reduced by NADH and oxidized by $AcPdAD^+$ (*28*). However, a combination of H_2NADH and $AcPdAD^+$ did not lead to any measurable cyclic transhydrogenation in dI_2dIII_1 complexes. This shows that H_2NADH cannot donate hydride equivalents to bound $NADP^+$ at a significant rate. In another set of experiments, isolated dIII (3 μM) in its $NADP^+$-bound form was preincubated with either 100 μM NADPH or 100 μM H_2NADPH for 2 h. This leads to exchange of the bound $NADP^+$ with either NADPH or H_2NADPH, respectively (see above). After then adding dI to generate dI_2dIII_1 complexes, cyclic transhydrogenation was assayed with NADH and $AcPdAD^+$. Where dIII had been preincubated with NADPH, the rate of the reaction was unabated, but where dIII had been preincubated with H_2-NADPH, it was slowed to 7% of the control rate (measured in complexes with bound $NADP^+$). Consistent with the stopped-flow data, these results suggest that bound H_2-NADPH cannot reduce $AcPdAD^+$; the low residual rate after preincubation with H_2NADPH can be attributed to $NADP^+$ that had not been exchanged from the complex.

There may be two reasons why H_2NADH and H_2NADPH are such poor hydride donors. First, their "enzyme-oxidized" forms (with H^- abstracted from $C4_N$) would have a 5,6-dihydronicotinamide ring (H_2Nic^+; see Scheme 1), which, unlike the nicotinamide ring of $NAD(P)^+$, is not stabilized by a delocalized π-electron system. The redox potential of the analogue couples will, therefore, be higher than that of $NAD(P)^+/NAD(P)H$ ($E_{m,7.0} \approx -0.32$ V), and H_2NADH and H_2NADPH will be weaker hydride donors (from $C4_N$) than their physiological equivalents. Second, there may be steric factors that prevent proper juxtaposition of the H_2NicH ring and the Nic^+ ring of the partner nucleotide at the hydride-transfer site. Thus, the extra hydrogen atoms at positions 5 and 6, the altered bond lengths of H_2NicH, and the greater tendency of the ring to pucker might interfere with the reaction geometry. The unchanged binding constant, at least for H_2NADH relative to NADH, perhaps argues against this, and an increased redox potential may be the predominant reason for the failure of the analogues to participate in hydride transfer.

The Formation of Dead-End dI_2dIII_1 Complexes Is Disfavored. In previous work, microcalorimetry experiments revealed two different NADH-binding sites on the dI_2dIII_1 complex (*52*). The K_d of one site (17 μM) was similar in value to that of isolated dI and was, therefore, assigned to the dI polypeptide in the complex [designated dI(A)] which,

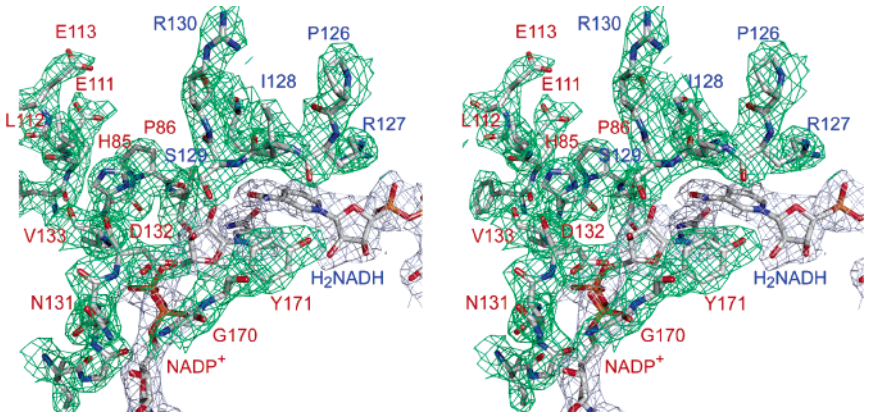

FIGURE 3: Electron density and atom coordinates of H_2NADH and NADP$^+$ at the interface between dI(B) and dIII in the dI_2dIII_1 complex (PDB 2OO5). The map (resolution 2.6 Å), shown in stereoview, is $2F_o - F_c$ contoured at 1σ. Electron densities of the nucleotides are shown in black, and those of amino acid residues are in green. Residues in dI are labeled in blue, and residues in dIII are in red.

in the crystal structure, makes few contacts with dIII (see Figure 4a). The K_d of the other site was elevated (to approximately 300 μM) and was assigned to the dI polypeptide, dI(B), which interacts strongly with dIII to form the hydride-transfer pocket. To block hydride transfer, which would otherwise have led to complicated heat changes, and thus to distortion of the K_d, these titrations were performed on dI_2dIII_1 complexes preloaded with NADPH rather than NADP$^+$ (apo-dIII from *R. rubrum* transhydrogenase is unstable). However, this left an ambiguity in the interpretation of the experimental result: it was not known whether the elevated K_d for NADH on dI(B) arose because dIII binding itself, or because the presence of the adjacent NADPH in the bound dIII, perturbed the site. Titrations with H_2NADH enable us to discriminate between the two possibilities. First, it was established that H_2NADH binds to NADPH-loaded dI_2dIII_1 complexes with parameters similar to those of NADH; there were indeed two binding sites, one with low (24 μM) and one with high (176 μM) K_d values (Figure S5a, Supporting Information). However, in subsequent H_2NADH titrations with NADP$^+$-loaded complexes (an experiment which is possible because the H_2NADH is redox-inactive), the results were quite different: the data could be fitted by a single class of binding site, $K_d = 44$ μM with a stoichiometry of 2.3 per dI_2dIII_1 complex (Figure S5b, Supporting Information). This suggests that perturbation by the nucleotide occupant of bound dIII, rather than dIII binding itself, has a more pronounced effect on the affinity of dI(B) for H_2NADH: bound NADPH lowers the binding affinity for H_2NADH (and presumably NADH) in dI(B). It seems that the dI_2dIII_1 complex can discriminate against the formation of dead-end species in which both bound nucleotides are reduced. A similar conclusion was drawn from experiments with the intact *E. coli* transhydrogenase when NADH binding to apoenzyme and to NADPH-loaded enzyme was compared (*85*).

Crystal Structures of dI_2dIII_1 Complexes. Samples of the dI_2dIII_1 complex loaded with NAD$^+$ and H_2NADPH crystallized under conditions similar to those described for the complex loaded with NADH and NADPH. Somewhat different conditions were required for the crystallization of complexes loaded with H_2NADH and NADP$^+$ (see Experimental Procedures). X-ray data sets for NAD$^+$/H_2NADPH complexes were processed and refined to 2.3 Å (PDB accession number 2OOR), and those for H_2NADH/NADP$^+$ complexes, to 2.6 Å (PDB 2OO5) (see Table 1). A $2F_o - F_c$ electron density map of the adjacent nicotinamide moieties of the bound H_2NADH and NADP$^+$ and their surrounding amino acid residues in 2OO5 is shown in Figure 3. An $F_o - F_c$ simulated annealing omit map of the region is presented in Figure S6 of the Supporting Information. Both 2OOR and 2OO5 have an essentially identical fold to that previously reported for the dead-end complexes (*32*, *33*). In each case, the structure comprises two dI polypeptides (A and B) and one dIII. The dIII is more closely associated with dI(B) than with dI(A) (see Figure 4a). The A and the B polypeptides of dI have slightly different conformations to one another but are related by a pseudo-2-fold axis. Each dI has two domains (dI.1 and dI.2) which are separated by a deep cleft. Most of the contact surface between the dI monomers is provided by the two dI.2 domains, but a distinctive β-hairpin extends from the dI.2 of each monomer to make contact with dI.1 of the symmetry-related partner (Figure 4b). The dIII component comprises a single domain and is located at one end of the cleft of dI(B). It makes extensive contacts with dI.2(B), although there is also an important contact region between the RQD loop (residues 126−136) of dI.1(B) and helix D/loop D (residues 131−155) of dIII. The polypeptide and domain nomenclature that we adopt for the dI_2dIII_1 complex is illustrated in Figure 4a.

Intact transhydrogenase has two hydride-transfer sites per dimer. However, dI_2dIII_1 complexes, typified by 2OOR and 2OO5, have only one, located at the dI(B)−dIII interface (see Figure 4c). The second hydride transfer site of the dI_2dIII_1 complex is incomplete because dI(A) is not associated with its own dIII (see below).

DISCUSSION

Detail at the Nucleotide-Binding Sites. To understand the mechanism of proton pumping by transhydrogenase, an accurate description of the hydride-transfer site is essential. In a first approach catalytically dead-end dI_2dIII_1 complexes were crystallized; the dI(B) nucleotide in structures with NAD$^+$/NADP$^+$ (1HZZ and 1U28) was disordered, but in a structure with NADH/NADPH (1U2D) the two NicH rings at the dI(B)−dIII interface were organized in a way that suggested we might have a good model for the hydride-transfer site (*32*, *33*). In a second approach dI_2dIII_1 complexes were crystallized in the presence of NADP$^+$ and excess

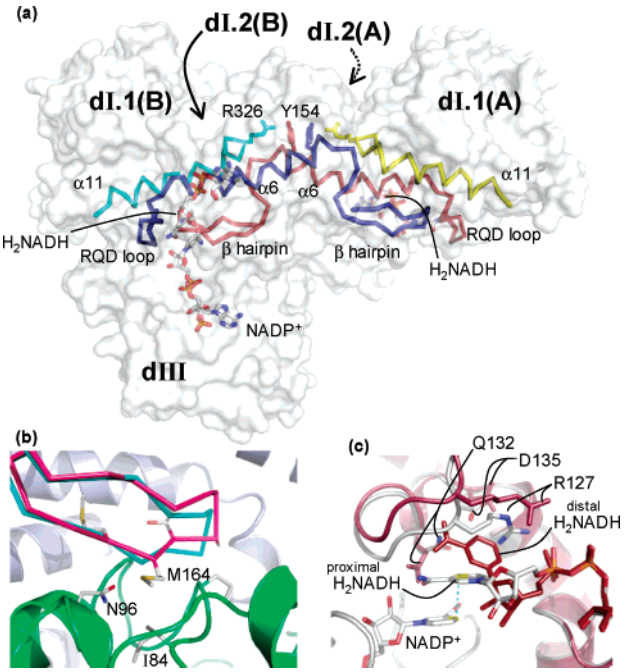

FIGURE 4: X-ray structure of the dI_2dIII_1 complex with bound H_2-NADH and $NADP^+$ (PDB 2OO5). (a) Surface model of the dI_2-$dIII_1$ complex, also showing the bound nucleotides (in their conventional atom colors) and the C_α traces of the RQD loop, helix α6, the *β*-hairpin, and helix α11 of the A and B polypeptides of dI. The figure shows the domain and polypeptide nomenclature used in the text. (b) Interaction between dIII and the *β*-hairpin of dI. The pale blue ribbons represent dI(B), and the green ribbons represent dIII. Shown in red is the C_α trace of the *β*-hairpin of dI(A) with the side chain of its Met164 making van der Waals contact with those of Ile84 and Asn96 in dIII. The cyan C_α trace shows how the *β*-hairpin of dI(B) models into this site when dI.2 of the A polypeptide is superposed onto that of the B polypeptide (at residues 202, 308, and 312; see Experimental Procedures); this leads to clashes between the Met164(B) and Ile84 and Asn96 in dIII. (c) The white polypeptide chains, and the side chains and nucleotides in conventional atom colors, show the hydride-transfer site at the interface between dI.1(B) and dIII. Here, the H_2NicH ring of the H_2NADH is proximal to the Nic^+ ring of the $NADP^+$. The dashed cyan line shows the apposition of the two $C4_N$ atoms (colored yellow). The amide group is shown with its O trans to $C2_N$ as discussed in the text. The side chains of Arg127, Gln132, and Asp135 of dI(B) are shown; they participate in an H-bonded network similar but not quite identical to that seen in the equivalent site of 1U2D (*33*). The brown polypeptide, amino acid side chains, and nucleotide are those of dI(A) modeled by superposing dI.2 of the A and B polypeptides, as described in (b). Here, the H_2NicH ring is distal, and side chain movements have led to disruption of the H-bonded network between Arg127, Gln132, and Asp135.

NADH; hydride transfer during crystallization led to the formation of NADH/NADPH dead-end complexes and to complexes with undefined nucleotide composition (1XLT) (*34*). The hydride-transfer site at the interface of dI(H)−dIII(I) of 1XLT is somewhat similar to that of dI(B)−dIII in 1U2D. In a third approach we have now crystallized dI_2-$dIII_1$ complexes with unreactive nucleotide/nucleotide analogue combinations having a charge distribution similar to those in the productive reactions with natural substrates. Thus, the charge distribution on the nucleotides bound in the blocked hydride-transfer site of 2OO5 (H_2NADH and $NADP^+$) is similar to that in the intermediate which precedes the redox reaction during forward transhydrogenation with natural substrates (NADH and $NADP^+$). The structure of the site in 2OO5 closely resembles that in 1U2D and somewhat resembles that in 1XLT. The convergence of the structures derived from the three different approaches strongly suggests that we have arrived at a reliable model for the hydride-transfer site of transhydrogenase. In 2OO5, which is at an improved resolution, the H_2NicH ring of the H_2NADH and the Nic^+ ring of the $NADP^+$ are aligned such that the two $C4_N$ atoms are apposed to one another (Figure 4c): the H_2-NicH ring of the H_2NADH is held in a proximal position relative to the $NADP^+$. This position is maintained by a network of H-bond interactions involving Gln132, Asp135, and Ser138 that hold Arg127 in a deep-lying location in the cleft between dI.1 and dI.2, preventing the H_2NicH from occupying a distal position (*33*, *86*, *87*). The site is sealed off from the solvent by the mobile loop (residues 220−240), whose Tyr235 also interacts with Arg127 and the nucleotide pyrophosphate. Note that the average *B*-factors for the bound H_2NADH (27.1 Å^2) and $NADP^+$ (36.1 Å^2), and those for the 32 amino acid residues lying within 5 Å of the nicotinamide mononucleotide moieties of these nucleotides (30.8 Å^2), are less than the average *B*-factor of the entire structure (40.7 Å^2), thus supporting the view that this is a stable conformation of the hydride-transfer site. If NADH is modeled in place of the H_2NADH in 2OO5, then the *pro-R* H on $C4_N$ is positioned to transfer to the $C4_N$ on the *si* face of $NADP^+$, that is, in agreement with the "A−B" hydride transfer determined experimentally (*2*, *3*).

The fact that both nucleotides are reduced in 1U2D and 1XLT (chains H and I) and that high concentrations of NADH are required to force occupation of the site in 1U2D (see above, Figure S5, and ref *52*) evidently does not lead to large-scale distortion. There are, however, small differences between the hydride-transfer sites of 2OO5 and those in the previously reported NADH/NADPH dead-end complexes. The two $C4_N$ atoms are separated by only 3.4 Å in 2OO5 compared with 3.6 Å in 1U2D and 4.6 Å in 1XLT (chains H and I), and the alignment of the (H_2)Nic(H) ring planes is slightly different in the three structures: in 2OO5 and in 1U2D the two ring planes are almost parallel (especially in 1U2D), but in 1XLT they are somewhat tilted. Furthermore, the H-bond network involving Arg127, Gln132, Asp135, and Ser138 of dI and the (H_2)Nic(H) pyrophosphate group adopts a slightly different pattern in 2OO5 and 1U2D and, particularly, in 1XLT. One striking difference is a flipped adenine position in 1XLT (chain H), not seen in any other dI polypeptide either in the isolated protein or in dI_2-$dIII_1$ complexes. It is not clear to what extent these differences are a consequence of the different resolutions of the structures (2.6 Å in 2OO5, 3.0 Å in 1U2D, and 3.1 Å in 1XLT) and to what extent they reflect real structural differences arising from the different states of nucleotide occupation.

The charge distribution on the nucleotides bound in the blocked hydride-transfer site of 2OOR (NAD^+ and H_2-NADPH) is similar to that in the intermediate which precedes the redox reaction during reverse transhydrogenation with natural substrates (i.e., NAD^+ and NADPH); see eq 1. However, the electron density for the NAD^+ in dI(B) of 2OOR is incomplete: that for the adenosine and pyrophosphate moieties of the nucleotide is clear but that for the Nic^+ ring is weak. This suggests at least moderate occupancy of the site by NAD^+, but disorder in the Nic^+ of the nucleotide that does bind, and contrasts with structures having bound

NADH where the electron density of the dI(B) nucleotide is clear (see above). The structure comparisons show that disorder in the bound NAD^+ of 1U28 is not simply a consequence of an unfavorable charge interaction between the Nic^+ rings of NAD^+ and $NADP^+$, as was previously suggested (*33*), because it is also evident (in 2OOR) where H_2NADPH (with its uncharged H_2NicH ring) is bound to dIII. It must be concluded that the poor density for Nic^+ in NAD^+-loaded structures is an intrinsic characteristic of the way in which this oxidized nucleotide binds to the dI component of the complex. Movement of the Nic(H) ring in the hydride-transfer site is thought to be an important feature of the transhydrogenase mechanism (see below). The greater disorder of the Nic^+ in bound NAD^+ than that of the NicH in bound NADH may signify a smaller population of nucleotide in the proximal state for hydride transfer during reverse transhydrogenation and thus partly explain the much lower (>36-fold) hydride-transfer rate in this direction (*88*).

In all published X-ray structures of dI_2dIII_1 complexes including those presented here there is bound nucleotide ($NADP^+$, NADPH, and H_2NADPH) in good electron density in the dIII polypeptide. Moreover, their conformations and those of neighboring amino acid residues are similar. The same is true of NADP(H) structures of isolated dIII, which are solved at higher resolution (*33*, *83*, *89*). Evidently, the changes in chemical shift that occur when $NADP^+$ is exchanged with either NADPH or H_2NADPH (Figure 2 and refs *54*, *82*, and *90*) are either predominantly electrostatic in origin or correspond to atomic displacements that are too small to be detected in X-ray structures at this resolution. The average coordinate error in 2OO5 is 0.4 Å as calculated from the Luzzati plot.

Molecular Dynamics Simulation of the Hydride-Transfer Site in dI_2dIII_1 Complexes. In the intact transhydrogenase interactions between the peripheral dI/dIII components and the membrane-spanning dII gate the hydride-transfer reaction and regulate the binding and release of NADP(H) (*8*−*11*). Isolated dI_2dIII_1 complexes are locked in a conformation in which the redox reaction can take place at rapid rates (*28*, *31*) and in which NADP(H) in dIII of dI_2dIII_1 complexes is occluded from the solvent by loop E (*26*). The X-ray structures of this complex are, therefore, a good model in which to study the protein dynamics of the intermediate state that is associated with hydride transfer in the intact enzyme. Figure 5 summarizes the results of an MD simulation of 2OO5 along a 1.4 ns trajectory. The average root mean square deviation of the C_α atoms indicates that the protein continues to sample conformations close to the X-ray structure across this time scale (Figure 5a). The H_2NicH ring of the H_2NADH and the Nic^+ ring of the $NADP^+$ remain close to parallel during the trajectory: the tilt between planes through the $C2_N$, $C4_N$, and $C6_N$ atoms of the two nucleotides in the time-averaged (0−1.4 ns) structure was 20.3° (compare 6.5° in 2OO5).

The distance between the $C4_N$ atoms of the H_2NicH and Nic^+ rings fluctuates between only very narrow limits (Figure 5b). The reason for this is apparent from the data shown in Figure 5c−g. Thus, relative movements of the rings perpendicular to their planes (Figure 5e,g) are small in comparison with relative movements within their planes (Figure 5c,d,f): fluctuations tend to slide the rings past each other but not separate them. Presumably, separation motions

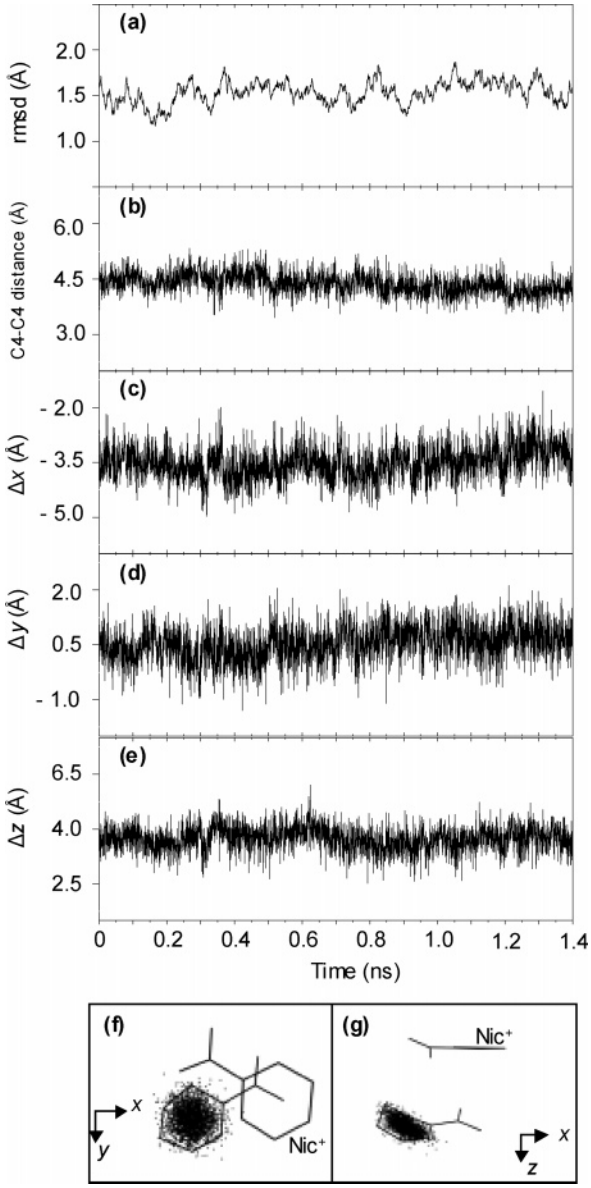

FIGURE 5: Molecular dynamics simulation of the dI_2dIII_1 complex, 2OO5. (a) Time dependence of the root mean square deviation (rmsd) of the protein C_α atoms relative to those of the energy-minimized starting structure. (b) Time dependence of the distance between $C4_N$ of the Nic^+ ring of $NADP^+$ and $C4_N$ of the H_2NicH ring of H_2NADH. (c−e) The $C2_N$, $C4_N$, and $C6_N$ atoms of the Nic^+ ring of the $NADP^+$ of each structure along the trajectory were superposed, and an $x-y$ plane was defined by the superposed atoms with an origin at the ring centers. The time dependence of the distance between the centers of the Nic^+ and H_2NicH rings along (c) the x coordinate, (d) the y coordinate, and (e) the z coordinate of the defined plane was determined from the superposed structures. (f, g) The lines show the projection of the Nic^+ and H_2NicH rings in the time-averaged structure, and the small dots show the positions of the center of the H_2NicH ring relative to that of the superposed Nic^+ rings of $NADP^+$ during the trajectory. The arrows indicate the directions of the x, y, and z coordinates: z is normal to the page in (f) and y is normal to the page in (g). Note that a parallel trajectory with different starting atomic velocities gave equivalent results to those shown in panels a−e.

(in the z-direction) are restrained by overlap of the π-electron systems of the two rings and their amide groups. As will be seen in the following section, the continued exploration of these apposed configurations of NicH and Nic^+ rings will readily lead to a reactive orientation for hydride transfer.

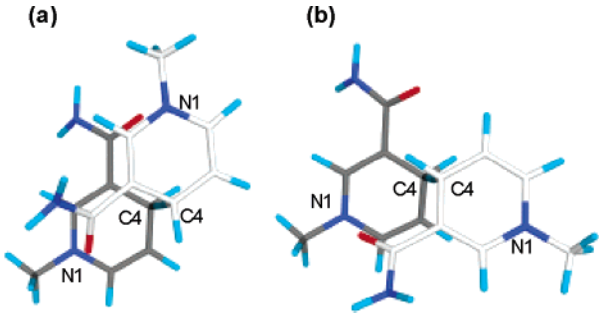

FIGURE 6: Transition-state structures of the hydride-transfer reaction between 1-methyl-1,4-dihydronicotinamide and the 1-methylnicotinamide cation. (a) Transition-state structure **1**. (b) Transition-state structure **7** (see Table S1). The C atoms of the upper ring are in white, and those of the lower ring are in gray. The transferred hydride can be just seen between the two C4 atoms in each structure.

The Transition State for Hydride Transfer between NAD(H) and NADP(H). Two transition-state structures for the C4−C4 hydride-transfer reaction between 1,4-dihydronicotinamide and protonated nicotinamide were identified by Wu et al. (*76*) using ab initio quantum mechanical methods (HF/6-31G*). Neither of these corresponds very well to the organization of the nicotinamide rings of nucleotides in the active site of transhydrogenase seen in the crystal structures. We have therefore extended the earlier calculations at a higher level of theory (dft/6-31G**), which includes a contribution for electron correlation. Furthermore, we have used 1-methyl analogues of dihydronicotinamide and protonated nicotinamide to provide a better model of the physiological reactants. Wu et al. (*76*) were working without the benefit of a crystal structure for this system and made the not unreasonable assumption that a symmetrical reaction (A + B → B + A) would pass through a symmetrical transition state (at least C_2). As the crystal structure shows a C_1 arrangement of nicotinamide rings, we did not follow this constraint. A number of possible transition states have been identified, including structures equivalent to those described (*76*) and all combinations of amide position and orientation based on the arrangement of dihydropyridine cores observed in the crystal structure. Their geometries and their total and relative energies are summarized in Table S1, and the two lowest energy structures, which differ by only 5.7 kJ mol^{-1}, are illustrated in Figure 6. Of all the calculated transition states, that with the second lowest energy (structure **7**; see Figure 6b) most resembles the organization of the H_2-NicH and Nic$^+$ rings of the H_2NADH and NADP$^+$ in the X-ray structure. Thus, in **7**, and in 2OO5, the planes of the two rings are close to parallel, the angle between the N1−C4 axes of the rings is approximately 120° (viewed from a normal to the ring planes as in Figure 6b), and while the C3−C7 bond of one amide group stacks on top of the C5−C6 bond of its partner ring, the other amide group points away from its respective partner. However, in the transition-state structure the two C4 atoms are in closer contact (2.67 Å), and both C4 atoms show partial sp^3 hybridization consistent with hydride transfer. The O atoms of each of the two amide groups in **7** are *trans* to C2 (though rotated slightly out of the ring plane). The transition-state structure **7** is asymmetric (it has C_1 symmetry), and unlike the C_2-symmetrical structure, **1**, it shows two different C4−H bond distances (1.29 and 1.38 Å compared with 1.34 Å, respectively). Asymmetric transition states for what is, in effect, a symmetrical reaction are highly unusual and are normally associated with a two-step mechanism that passes through a symmetrical intermediate. That is clearly not the case here as both frequency and IRC calculations confirm that this structure is a first-order transition state for hydride transfer occurring as a single step. Transition-state structures **9** and **10** are similar to **7** but have the O atom of one amide *cis* to its C2; this raises the energy of the transition state by approximately 20 and 6 kJ mol^{-1}, respectively, possibly for the reasons put forward (*76*). Transition-state structure **8** has both amide O atoms *cis* to their C2s, and its energy is elevated by approximately 20 kJ mol^{-1}. The resolution of the X-ray structure is not enough directly to identify the rotation of the amide group about the C3−C7 bond, but the H-bonding pattern indicates that the O is *trans* to C2 in the amide of NADP$^+$; equivalent clues are unfortunately lacking for the H_2NADH, and thus the crystal structure could correspond to either transition state **7** or **10** but not to either **8** or **9**. The possible significance of amide rotation in transhydrogenase turnover was discussed (*89*).

The similarity between the X-ray structure and a low-energy transition state may indicate that the transhydrogenase active site has evolved to optimize the relative positions of the Nic(H) rings and thus favor a rapid rate of hydride transfer from bound NADH to NADP$^+$. For efficient coupling to proton translocation through the enzyme, there is also a need to switch on and switch off hydride transfer by moving the Nic(H) ring of the NAD(H) at appropriate times in the reaction cycle (see refs *33* and *86* and below). It would seem that this requirement has been managed during evolution without significantly compromising the need for an optimized position of the Nic(H) rings that will lead to a rapid redox reaction at the point of hydride transfer.

Coupled Asymmetric Motions in the dI Dimer: The Role of the β-Hairpin in the Asymmetric Binding of dIII. In the dI(A) polypeptides of all published wild-type dI$_2$dIII$_1$ structures the electron density of bound nucleotide is very clear, and the NAD(H) is seen to adopt a distinctively different conformation to that of NAD(H) in the dI(B)−dIII hydride-transfer site. The same is true for the NAD$^+$ in dI(A) of 2OOR and for the H_2NADH in dI(A) of 2OO5, giving further support to the notion that the binding of the tetrahydro analogues leads to conformational changes similar to those resulting from the binding of physiological nucleotides. Thus, whatever the redox state, the nicotinamide moiety in all dI(A) polypeptides is pushed further back into the cleft between dI.1 and dI.2 than in dI(B). There are accompanying changes in the side chain conformations and H-bonding pattern of Arg127, Gln132, Asp135, and Ser138 in the RQD loop, and these share similar features in all structures and appear to be responsible for holding the nucleotide position (*33*, *86*, *87*). If the NAD(H) conformation seen in dI(A) were adopted in the dI(B)−dIII hydride-transfer site, the C4$_N$ atom of the nucleotide would be too far from that of bound NADP(H) to allow the redox reaction (*32*, *33*). This position of the Nic(H) was therefore described as distal, and a role for the distal−proximal switch in the gating of hydride transfer was suggested.

There are other asymmetric features in the A and B polypeptides of dI. Notably, these include a different degree of rotation of domains dI.1 and dI.2 and a different position of the β-hairpin. An analysis of the available structures as

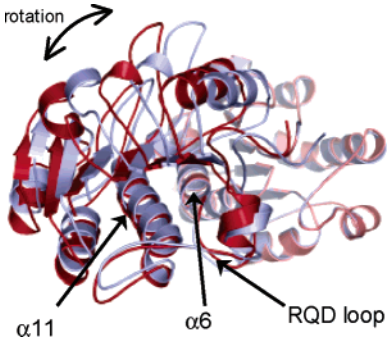

FIGURE 7: Difference in the relative rotation of the dI.1 and dI.2 domains between the A and B polypeptides of the dI_2dIII_1 complex, 2OO5. The C_α of residues 202, 308, and 312 of the dI.2 domain of the A polypeptide were superposed on the equivalent atoms of the B polypeptide (as described in Figure 4). The A polypeptide is in red, and the B polypeptide is in blue. The view is orthogonal to, and from the left of, that in Figure 4a. Thus, the dI.1 domains are at the front, and the dI.2 domains are superposed at the back.

outlined below and a consideration of recent work on a β-hairpin mutant (*24*) suggest that the asymmetries reflect structural changes that occur during operation of the enzyme. Specifically, we propose that these changes are involved in controlling the alternating interactions between dI and dIII at the two hydride-transfer sites.

There is a difference in the relative rotation of domains dI.1 and dI.2 in the two monomers of the dimer in crystals of isolated dI (*22*, *23*). The axis of the rotation lies approximately along α helices 6 and 11 which link the two domains (see Figure 4a). There is an equivalent difference in the relative rotation of dI.1 and dI.2 in dI(A) and dI(B) in dI_2dIII_1 complexes (refs *32*, *33*, and *89* and this work). Importantly, this always has the same sense in dI(B), which binds dIII, relative to that in dI(A), which does not. The relative rotation between dI.1 and dI.2 in A and B of 2OO5 is approximately 9° and is illustrated in Figure 7 and on the MORPH server (code 031760-24674) (*64*). In contrast, there are no detectable relative movements between the dI.2 domains of the A and B polypeptides; these appear to form a central core for the rotations of the peripheral dI.1 domains. It is concluded that the rotations of dI.1 and dI.2 are coupled and reciprocating and that dIII binds more tightly to the dI monomer that has the rotation found in the B polypeptide.

Figure 4b indicates that movements of the β-hairpin, residues 157−175 in dI, may be responsible for this binding selection. The β-hairpin of dI(A) extends around the contact site between dI(B) and dIII and allows a favorable interaction. However, the β-hairpin of dI(B) is in a different position, and this obstructs the docking of a dIII polypeptide onto dI-(A). The positional change is small (1−2 Å at the β-turn of the hairpin) but can be seen in structures 1HZZ, 1U2D, 2OOR, and 2OO5 of the dI_2dIII_1 complex and in 1F8G and 1L7E of the isolated dI dimer (not shown). It involves a hinged motion about residues Ala157 and Val175. The direction of the β-hairpin movement correlates with the direction of rotation of dI.1 and dI.2 indicating a linkage. Note that each β-hairpin makes extensive contact with the dI.1 of its symmetry-related partner polypeptide. It is suggested, therefore, that the domain rotations cause the change in β-hairpin position alternately to enable and to prevent the binding of dIII.

The role of the β-hairpin has also aroused the interest of other workers. Johansson et al. (*24*) recently constructed a mutant of *E. coli* dI carrying a 10-residue deletion in this element. The mutant protein folded as a dimer, had an affinity for *E. coli* dIII similar to wild-type dI, and the resulting complex had only a slightly decreased rate of hydride transfer. The similar affinity between dIII and mutant dI was thought to be "surprising" (*24*) because the β-hairpin contributes to the dI−dIII contact surface (*32*). In fact, these findings are entirely consistent with the suggestion advanced above: the β-hairpin is not required to promote dIII binding but rather to prevent it at the appropriate step in alternating-site catalysis. In the reported experiments (*24*) we infer that dIII will bind to either of the polypeptides (A or B) in the mutant dI to give a complex capable of good rates of hydride transfer; in contrast, dIII will bind only to dI(B) of wild-type dI. It is expected that a β-hairpin deletion in the intact enzyme (as distinct from dI−dIII complexes) would disrupt proton-translocating transhydrogenation.

How the reciprocating rotations of dI.1 and dI.2 in the A and B polypeptides are coupled is not yet understood. Nevertheless, the rotations seem to drive positional changes in the RQD loop, which shift the Nic(H) rings of bound NAD(H) between proximal and distal conformations to enable or block hydride transfer, as described (*33*, *86*, *87*) and, simultaneously, lead to changes in the β-hairpin position, which either enable or inhibit the binding of dIII. Because the rotations are reciprocating, the events in the A and B monomers are 180° out of phase in accordance with the "alternating-site" model of proton pumping by transhydrogenase (*21*, *32*). It is widely accepted (following ref *8*) that proton translocation through dII results in conformational changes, which manifest as NADP(H)-binding changes in dIII (*6*, *7*, *9*−*11*). The conformational changes in dI described above are subordinate to the conformational events in dII and dIII that are driven by proton translocation. The nature of these long-distance conformational changes is a matter of great interest.

The Structure of dI−dIII Complexes versus Crystal Packing. Recently, a previously unreported interaction between *R. rubrum* dI and dIII was described (*34*). In addition to the interactions discussed (*32*, *33*) (and see above), it was observed that there is another contact surface in the crystal lattice of the dIdIII structure, 1XLT. This surface is between dI and the face of dIII opposite to that housing the NADP-(H)-binding site (see Figure 8a). It was suggested that the interaction is not a crystallographic artifact but that it reflects a real contact surface in a hitherto unrecognized state of the intact enzyme; in this state, the NADP(H)-binding site of dIII would be brought into contact with the membrane-spanning dII. During catalysis, the entire dIII component would rotate by 180° between the originally described (*32*, *33*) and the newly described (*34*) structural states. Were this to be true, it would represent an important new development in our understanding of transhydrogenase. However, in our view there is a distinct possibility that the "new" contact surface does only arise from crystal packing and that it does not reflect interactions either in the solution state of the dI_2-$dIII_1$ complex or in the intact enzyme.

The first reason to be skeptical about additional contacts between dI and dIII is that in stopped-flow, ultracentrifuge, microcalorimetry, and low-angle X-ray scattering experi-

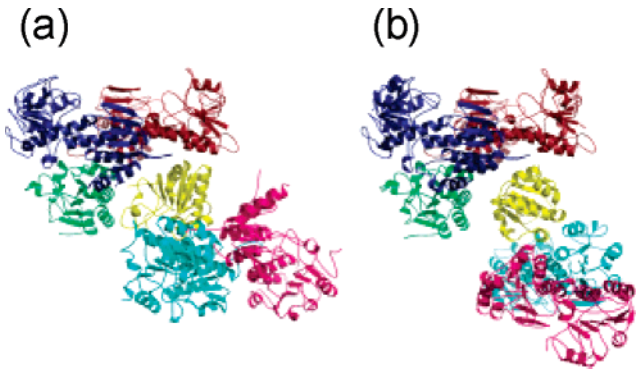

FIGURE 8: Crystal lattice contacts in the dI_2dIII_1 complex of 1XLT and 2OO5. (a) The brown polypeptide is dI(G), the blue is dI(H), and the green is dIII(I) of 1XLT (*34*). This organization is similar to that of the dI_2dIII_1 complex derived from the earlier crystal forms, 1HZZ (*32*) and 1U2D (*33*), and is shown from the same perspective as in Figure 4a of this report. Also depicted are polypeptides dI(A) in pink, dI(B) in cyan, and dIII(C) in yellow, which form another dI_2dIII_1 complex in the unit cell (*34*). The yellow dIII(C) polypeptide is seen to make contacts with the brown dI(G) and the green dIII(I). (b) The brown polypeptide is dI(A), the blue is dI(B), and the green is dIII of 2OO5, shown from the same perspective as G, H, and I of 1XLT in panel a. Another dI_2dIII_1 complex from the crystal lattice of 2OO5 (related by $x + {}^1/_2$, $-y - {}^1/_2$, $-z$ crystallographic symmetry) is shown with dI polypeptides in pink and cyan and dIII in yellow. Again, there are contacts between the yellow dIII and the brown dI/green dIII, but note the different orientation of the yellow dIII polypeptides in (a) and (b).

ments it was established that the complex of dI and dIII, in solution, has a dI_2dIII_1 stoichiometry (*30*, *52*). The K_d for the binding of the dI dimer to the dIII monomer is <60 nM. NMR experiments in the solution state show that a second dIII can bind to the dI_2dIII_1 complex but with a K_d that is >3 orders of magnitude higher than the first (*54*). Importantly, the distribution of chemical shift perturbations of amino acid side chains indicates that the second dIII binds to dI(A) in a manner that is roughly equivalent to the binding of the first dIII to dI(B); there were no chemical shift perturbations that can be attributed to an "inverted" binding of dIII.

A second reservation concerning the putative inverted contact between dI and dIII (*34*) is that there is an analogous but, in detail, distinctively quite different interaction between dI and dIII evident in the earlier structures of dI_2dIII_1 (PDB 1HZZ, 1PT9, 1U28, 1U2D) and in 2OOR and 2OO5 reported here. In all of these structures there is, in the crystal lattice, a contact surface between dI and the face of dIII opposite to the nucleotide-binding site although, significantly, this is twisted approximately 90° relative to that described in 1XLT; the contact surface in 2OO5 is shown in Figure 8b. The contact is very clear in the earlier published data, but because of the biophysical data (see above), we had privately attributed it to a crystal-packing artifact and rejected the idea that it is a significant structural feature. Following the logic of ref *34*, it could alternatively be concluded that this contact is also real and that it too reflects an intermediate state during turnover of the intact enzyme. However, we should then arrive at the notion that, during catalysis, dIII undergoes two consecutive rotations on orthogonal axes. This is implausible not least because it is doubtful if the polypeptide linking dII and III is flexible enough to allow both sets of motions. It is also pertinent that transhydrogenases from protozoan parasites have a structure similar to bacterial and mammalian enzymes, but they are joined, not only by a polypeptide linker between dII and dIII but also by a linker between dIII and dI (*91*−*94*). Even one set of rotational movements of the kind described (*34*) would present a formidable problem of polypeptide topology for these enzymes, which appear to operate by a mechanism similar to that of the bacterial and mammalian transhydrogenases (*95*, *96*).

A final reason to be cautious about the inverted binding of dIII in the X-ray structures is that it is difficult to understand what feature of the enzyme mechanism would be favored by rotating the NADP(H) site, with its bound nucleotide, into the membrane domain. Whether or not there are large subunit rearrangements that take place during transhydrogenase turnover remains an important question, although good evidence for such changes is still lacking.

ACKNOWLEDGMENT

We are grateful to Dr. Alan Cooper and Margaret Nutley (University of Glasgow), Francois Dupradeau (University of Picardie), Phil Evans (University of Cambridge), Nick Cotton, Gijs van Boxel, Owen Mather, Harma Brondijk, Klaus Futterer, and Paul Simpson (University of Birmingham), and the staff at the European Radiation Facility at Grenoble for help and advice.

SUPPORTING INFORMATION AVAILABLE

Table S1, energies and schematic structures of hydride-transfer transition states; Figure S1, quenching of Trp72 fluorescence of isolated dI by H_2NADH; Figure S2, heat changes during titrations of isolated dI with H_2NADH; Figure S3, chemical shift changes of Met239 in the mobile loop of isolated dI induced by H_2NADH; Figure S4, effect of H_2NAD(P)H on reverse transhydrogenation in chromatophore membranes; Figure S5, heat changes during titrations of dI_2dIII_1 complexes with H_2NADH and NADH; Figure S6, electron density omit map of the hydride-transfer site in 2OO5. This material is available free of charge via the Internet at http://pubs.acs.org.

REFERENCES

1. Venning, J. D., Grimley, R. L., Bizouarn, T., Cotton, N. P. J., and Jackson, J. B. (1997) Evidence that the transfer of hydride equivalents between nucleotides by proton-translocating transhydrogenase is direct, *J. Biol. Chem. 272*, 27535−27538.
2. Lee, C. P., Simard-Duquesne, N., Ernster, L., and Hoberman, H. D. (1965) Stereochemistry of hydrogen transfer in the energy-linked pyridine nucleotide transhydrogenase and related reactions, *Biochim. Biophys. Acta 105*, 397−409.
3. Griffiths, D. E., and Roberton, A. M. (1966) Energy-linked reactions in mitochondria: studies on the mechanism of the energy-linked transhydrogenation reaction, *Biochim. Biophys. Acta 118*, 453−464.
4. Bizouarn, T., Sazanov, L. A., Aubourg, S., and Jackson, J. B. (1996) Estimation of the H^+/H^- ratio of the reaction catalysed by the nicotinamide nucleotide transhydrogenase in chromatophores from over-expressing strains of *Rhodospirillum rubrum* and in liposomes inlaid with the purified bovine enzyme, *Biochim. Biophys. Acta 1273*, 4−12.
5. Jackson, J. B., White, S. A., and Brondijk, T. H. C. (2005) Hydride transfer and proton translocation by nicotinamide nucleotide transhydrogenase, in *Biophysical and Structural Aspects of Bioenergetics* (Wikstrom, M., Ed.) pp 376−393, Royal Society of Chemistry, Cambridge.
6. Bizouarn, T., Fjellstrom, O., Meuller, J., Axelsson, M., Bergkvist, A., Johansson, C., Karlsson, G., and Rydstrom, J. (2000) Proton translocating nicotinamide nucleotide transhydrogenase from *E.*

coli. Mechanism of action deduced from its structural and catalytic properties, *Biochim. Biophys. Acta 1457*, 211−218.
7. Hatefi, Y., and Yamaguchi, M. (1996) Nicotinamide nucleotide transhydrogenase: a model for utilization of substrate binding energy for proton translocation, *FASEB J. 10*, 444−452.
8. Hutton, M. N., Day, J. M., Bizouarn, T., and Jackson, J. B. (1994) Kinetic resolution of the reaction catalysed by proton-translocating transhydrogenase from *Escherichia coli* as revealed by experiments with nucleotide substrate analogues, *Eur. J. Biochem. 219*, 1041−1051.
9. Bragg, P. D., and Hou, C. (2001) Characterisation of mutants of beta-histidine91, beta-aspartate213 and beta-asparagine222, possible components of the energy-transduction pathway of the proton-translocating pyridine nucleotide transhydrogenase of *Escherichia coli*, *Arch. Biochem. Biophys. 388*, 299−307.
10. Yamaguchi, M., and Stout, C. D. (2003) Essential glycine residues in the proton channel of *Escherichia coli* transhydrogenase, *J. Biol. Chem. 278*, 45333−45339.
11. Karlsson, J., Althage, M., and Rydstrom, J. (2003) Roles of individual amino acid in helix 14 of the membrane domain of proton-translocating transhydrogensae from *Escherichia coli* as deduced from cysteine mutagenesis, *Biochemistry 42*, 6575−6581.
12. Oshino, N., and Chance, B. (1977) Properties of glutathione release observed during reduction of organic hydroperoxide, demethylation of aminopyridine and oxidation of some substances in perfused rat liver, and their implications for the physiological function of catalase, *Biochem. J. 162*, 509−525.
13. Rydstrom, J., and Hoek, J. B. (1988) Physiological roles of nicotinamide nucleotide transhydrogenase, *Biochem. J. 254*, 1−10.
14. Sazanov, L. A., and Jackson, J. B. (1994) Proton translocating transhydrogenase and NAD- and NADP-linked isocitrate dehydrogenases operate in a substrate cycle which contributes to the fine regulation of the tricarboxylic acid cycle activity in mitochondria, *FEBS Lett. 344*, 109−116.
15. Ambartsoumian, G., Dari, R., Lin, R. T., and Newman, E. B. (1994) Altered amino-acid metabolism in LRP mutants of *Escherichia coli* K12 and their derivatives, *Microbiology 140*, 1737−1744.
16. Hickman, J. W., Barber, R. D., Skaar, E. P., and Donohue, T. J. (2002) A link between the membrane-bound pyridine nucleotide transhydrogenase and glutathione-dependent processes in *Rhodobacter sphaeroides*, *J. Bacteriol. 184*, 400−409.
17. Arkblad, E. L., Tuck, S., Pestov, N. B., Dmitriev, R. I., Kostina, M. B., Stenvall, J., Tranberg, M., and Rydstrom, J. (2005) A *Caenorhabditis elegans* mutant lacking functional nicotinamide nucleotide transhydrogenase displays increased sensitivity ot oxidative stress, *Free Radical Biol. Med. 38*, 1518−1525.
18. Freeman, H., Shimomura, K., Horner, E., Cox, R. D., and Ashcroft, F. M. (2006) Nicotinamide nucleotide transhydrogenase: a key role in insulin secretion, *Cell. Metab. 3*, 35−45.
19. Meuller, J., and Rydstrom, J. (1999) The membrane topology of proton-pumping *Escherichia coli* transhydrogenase determined by cysteine labelling, *J. Biol. Chem. 274*, 19072−19080.
20. Wilson, R., Obiozo, U. M., Quirk, P. G., Besra, G. D., and Jackson, J. B. (2006) A hybrid of the transhydrogenases from *Rhodospirillum rubrum* and *Mycobacterium tuberculosis* catalyses rapid hydride transfer but not the complete, proton-translocating reaction., *Biochim. Biophy. Acta 1537*, 215−223.
21. Jackson, J. B., White, S. A., Quirk, P. G., and Venning, J. D. (2002) The alternating site, binding change mechanism for proton translocation by transhydrogenase, *Biochemistry 41*, 4173−4185.
22. Buckley, P. A., Jackson, J. B., Schneider, T., White, S. A., Rice, D. W., and Baker, P. J. (2000) Protein-protein recognition, hydride transfer and proton pumping in the transhydrogenase complex, *Structure 8*, 809−815.
23. Prasad, G. S., Wahlberg, M., Sridhar, V., Sundaresan, V., Yamaguchi, M., Hatefi, Y., and Stout, C. D. (2002) Crystal structures of transhydrogenase domain I with and without bound NADH, *Biochemistry 41*, 12745−12754.
24. Johansson, T., Oswald, C., Pedersen, A., Tornroth, S., Okvist, M., Karlsson, B. G., and Rydstrom, J. (2005) X-ray structure of domain I of the proton-pumping membrane protein transhydrogenase from *Escherichia coli*, *J. Mol. Biol. 352*, 299−312.
25. Prasad, G. S., Sridhar, V., Yamaguchi, M., Hatefi, Y., and Stout, C. D. (1999) Crystal structure of transhydrogenase domain III at 1.2 Å resolution, *Nat.e Struct. Biol. 6*, 1126−1131.
26. White, S. A., Peake, S. J., McSweeney, S., Leonard, G., Cotton, N. N. J., and Jackson, J. B. (2000) The high resolution structure of the NADP(H)-binding component of proton-translocating transhydrogenase from human-heart mitochondria, *Structure 8*, 1−12.
27. Jeeves, M., Smith, K. J., Quirk, P. G., Cotton, N. P. J., and Jackson, J. B. (2000) Solution structure of the NADP(H)-binding component (dIII) of proton-translocating transhydrogenase from *Rhodospirillum rubrum*, *Biochim. Biophys. Acta 1459*, 248−257.
28. Diggle, C., Bizouarn, T., Cotton, N. P. J., and Jackson, J. B. (1996) Properties of the purified, recombinant, NADP(H)-binding domain III of the proton-translocating nicotinamide nucleotide transhydrogenase from *Rhodospirillum rubrum*, *Eur. J. Biochem. 241*, 162−170.
29. Yamaguchi, M., and Hatefi, Y. (1997) High cyclic transhydrogenase activity catalysed by expressed an reconstituted nucleotide-binding domains of *Rhodospirillum rubrum* transhydrogenase, *Biochim. Biophys. Acta 1318*, 225−234.
30. Venning, J. D., Bizouarn, T., Cotton, N. P. J., Quirk, P. G., and Jackson, J. B. (1998) Stopped-flow kinetics of hydride transfer between nucleotides by recombinant domains of proton-translocating transhydrogenase, *Eur. J. Biochem. 257*, 202−209.
31. Venning, J. D., Peake, S. J., Quirk, P. G., and Jackson, J. B. (2000) Stopped-flow reaction kinetics of recombinant components of proton-translocating transhydrogenase with physiological nucleotides, *J. Biol. Chem. 275*, 19490−19497.
32. Cotton, N. P. J., White, S. A., Peake, S. J., McSweeney, S., and Jackson, J. B. (2001) The crystal structure of an asymmetric complex of the two nucleotide-binding components of proton-translocating transhydrogenase, *Structure 9*, 165−176.
33. Mather, O. M., van Boxel, G. I., White, S. A., and Jackson, J. B. (2004) Active-site conformational changes associated with hydride transfer in proton-translocating transhydrogenase, *Biochemistry 43*, 10952−10964.
34. Sundaresan, V., Chartron, J., Yamaguchi, M., and Stout, C. D. (2005) Conformational diversity in NAD(H) and interacting transhydrogenase nicotinamide nucleotide binding domains, *J. Mol. Biol. 346*, 617−629.
35. Biellman, J. F., and Jung, M. J. (1971) Mechanism of the alcohol dehydrogenase from yeast and horse liver, *Eur. J. Biochem 19*, 130−134.
36. Olomucki, A., Thome-Beau, F., Biellman, J. F., and Branlant, G. (1975) Study of coenzyme binding site of octupine dehydrogenase using analogues of NAD^+, *Eur. J. Biochem 56*, 116.
37. Thevenot, D. R., Godinot, C., Gautheron, D. C., Branlant, G., and Biellman, J. F. (1975) Binding of L-glutamate to glutamate dehydrogenase in the presence of 1,4,5,6-tetrahydronicotinamide adenine dinucleotide, *FEBS Lett. 54*, 206−211.
38. Biellman, J. F., and Hirth, C. G. (1975) $NAD(P)^+$ analogues: tools for the investigation of the active site of oestradiol 17-beta-dehydrogenase from human placenta, *Eur. J. Biochem. 56*, 557−561.
39. Dunn, M. F., Biellman, J. F., and Branlant, G. (1975) Roles of zinc ion and reduced coenzyme in horse liver alcohol dehydrogenase catalysis. The mechanism of aldehyde activation, *Biochemistry 14*, 3176−3182.
40. Cedergren-zeppenauer, E., Samama, J.-P., and Eklund, H. (1982) Crystal structure determinations of coenzyme analogue and substrate complexes of liver alcohol dehydrogenase: binding of 1,4,5,6-tetrahydronicotinamide adenine dinucleotide and *trans*-4-(*N*,*N*-dimethylamino)cinnamaldehyde to the enzyme, *Biochemistry 21*, 4895−4908.
41. Chapman, A. D. M., Cortes, A., Dafforn, T. R., Clarke, A. R., and Brady, R. L. (1999) Structural basis of substrate specificity in malate dehydrogenses: crystal structure of a ternary complex of porcine cytoplasmic malate dehydrogenase, alpha-ketomalonate and tetrahydroNAD, *J. Mol. Biol. 285*, 703−712.
42. Weaver, P. F., Wall, J. D., and Gest, H. (1975) Characterisation of *Rhodopseudomonas capsulata*, *Arch. Microbiol. 105*, 207−216.
43. Cunningham, I. J., Williams, R., Palmer, T., Thomas, C. M., and Jackson, J. B. (1992) The relation between the soluble factor associated with H^+-transhydrogenase of *Rhodospirillum rubrum* and the enzyme from mitochondria and *Escherichia coli*, *Biochim. Biophys. Acta 1100*, 332−338.
44. Clayton, R. K. (1963) Towards the isolation of a photochemical reaction centre in *Rhodopseudomonas capsulata*, *Biochim. Biophys. Acta 73*, 312−323.
45. Diggle, C., Hutton, M., Jones, G. R., Thomas, C. M., and Jackson, J. B. (1995) Properties of the soluble polypeptide of the proton-

translocating transhydrogenase from *Rhodospirillum rubrum* obtained by expression in *Escherichia coli*, *Eur. J. Biochem. 228*, 719−726.
46. Jeeves, M., Smith, K. J., Quirk, P. G., Cotton, N. P. J., and Jackson, J. B. (1999) Sequence-specific resonance assignments for the NADP(H)-binding component (domain III) of proton-translocating transhydrogenase from *Rhodospirillum rubrum*, *J. Biomol. NMR 13*, 305−306.
47. Peake, S. J., Venning, J. D., Cotton, N. P. J., and Jackson, J. B. (1999) Evidence for the stabilization of NADPH relative to $NADP^+$ in the dIII components of proton-translocating transhydrogenase from *Homo sapiens* and from *Rhodospirillum rubrum* by measurement of tryptophan fluorescence, *Biochim. Biophys. Acta 1413*, 81−91.
48. Mejbaum-Katzenellenbogen, S., and Drobryszycka, W. J. (1959) New methods for quantitative determination of serum proteins separated by paper chromatography, *Clin. Chim. Acta 4*, 515−522.
49. Dave, K. G., Dunlap, R. B., Jain, M. K., Cordes, E. H., and Wenkert, E. (1968) Highly reduced analogues of the pyridine nucleotides, *J. Biol. Chem. 243*, 1073−1074.
50. Branlant, G., Eiler, B., and Biellman, J. F. (1982) A word of caution: 1,4,5,6-tetrahydronicotinamideandenine dinucleotide (phosphate) should be used with care in acidic and neutral media, *Anal. Biochem. 125*, 264−268.
51. Palmer, T., and Jackson, J. B. (1992) Nicotinamide nucleotide transhydrogenase from *Rhodobacter capsulatus*; the H^+/H^- ratio and the activation state of the enzyme during reduction of acetyl pyridine adenine dinucleotide, *Biochim. Biophys. Acta 1099*, 157−162.
52. Venning, J. D., Rodrigues, D. J., Weston, C. J., Cotton, N. P. J., Quirk, P. G., Errington, N., Finet, S., White, S. A., and Jackson, J. B. (2001) The heterotrimer of the membrane-peripheral components of transhydrogenase and the alternating-site mechanism of proton translocation, *J. Biol. Chem. 276*, 30678−30685.
53. Diggle, C., Cotton, N. P. J., Grimley, R. L., Quirk, P. G., Thomas, C. M., and Jackson, J. B. (1995) Conformational dynamics of a mobile loop in the NAD(H)-binding subunit of proton-translocating transhydrogenases from *Rhodospirillum rubrum* and *Escherichia coli*, *Eur. J. Biochem. 232*, 315−326.
54. Quirk, P. G., Jeeves, M., Cotton, N. P. J., Smith, K. J., and Jackson, J. B. (1999) Structural changes in the recombinant, NADP(H)-binding component (dIII) of proton-translocating transhydrogenase revealed by NMR spectroscopy, *FEBS Lett. 446*, 127−132.
55. Kraulis, P. J. (1989) ANSIG: A program for the assignment of protein ^{1}H 2D NMR spectra by interactive graphics, *J. Magn. Reson. 24*, 627−633.
56. Rajesh, S., Sakamoto, T., Iwamoto-Sugai, M., Shibata, T., Hohno, T., and Ito, Y. (1999) Ubiquitin binding interface mapping on yeast ubiquitin hydrolase by NMR chemical shift perturbation, *Biochemistry 38*, 9242−9253.
57. Leslie, A. G. W. (1992) Recent changes to the MOSFLM package for processing film and image data, *Jt. CCCP4 ESF-EADBM Newsl. Protein Crystallogr. 226*.
58. Evans, P. R. (1997) SCALA, *Jt. CCP4 ESF-EACMB Newsl. 33*, 22−24.
59. Kissinger, C. R., Gelhaar, D. K., and Fogel, D. B. (1999) Rapid automated molecular replacement by evolutionary search, *Acta Crystallogr.* D55, 484−491.
60. Murshudov, G. N., Vagin, A. A., and Dodson, E. J. (1997) REFMAC5, *Acta Crystallogr. D 53*, 240−255.
61. Brunger, A. T., Adams, P. D., Clore, G. M., Delano, W. L., Gros, P., Grossekunstleve, R. W., Et, A. L., and Warren, G. L. (1998) Crystallography and NMR system: A new software suite for macromolecular structure determination, *Acta Crystallogr. D 54*, 905−921.
62. Hooft, R. W. W., Vriend, G., Sander, C., and Abola, E. E. (1996) Errors in protein structures, *Nature 381*, 272.
63. Laskowski, R. A., Macarthur, M. W., Moss, D. S., and Thornton, J. M. (1993) PROCHECK: a programme to check the stereochemical quality of protein structures, *J. Appl. Crystallogr. 26*, 283−291.
64. Krebs, W. G., and Gerstein, M. (2000) The MORPH server: a standardized system for analyzing and visualizing macromolecular motions in a database framework, *Nucleic Acids Res. 28*, 1665−1675.
65. Case, D. A., Darden, T. A., Cheatham, I. T. E., Simmerling, C. L., Wang, J., Duke, R. E., Luo, R., Merz, K. M., Wang, B., Pearlman D. A., Crowley, M., Brozell, S., Tsui, V., Gohlke, H., Mongan, J., Hornak, V., Cui, G., Beroza, P., Schafmeister, C., Caldwell, J. W., Ross, W. S., and Kollman P. A. (2004) Amber8, University of California, San Francisco.
66. Holmberg, N., and Ryde, U. (2006) Redesign of the coenzyme specificity in L-lactate dehydrogenase from *Bacillus stearothermophilus* using site-directed mutagenesis and media engineering, *Protein Eng. 12*, 851−856.
67. Frisch, M. J., Trucks, G. W., Schlegel, H. B., Scuseria, G. E., Robb, M. A., Cheeseman, J. R., Zakrzewski, V. G., Montgomery, J. A., Jr., Stratmann, R. E., Burant, J. C., Dapprich, S., Millam, J. M., Daniels, A. D., Kudin, K. N., Montgomery, J. A., Jr., Stratmann, R. E., Burant, J. C., Dapprich, S., Millam, J. M., Daniels, A. D., Kudin, K. N., Strain, M. C., Farkas, O., Tomasi, J., Barone, V., Cossi, M., Cammi, R., Mennucci, B., Pomelli, C., Adamo, C., Clifford, S., Ochterski, J., Petersson, G. A., Ayala, P. Y., Cui, Q., Morokuma, K., Malick, D. K., Rabuck, A. D., Raghavachari, K., Foresman, J. B., Cioslowski, J., Ortiz, J. V., Stefanov, B. B., Liu, G., Liashenko, A., Piskorz, P., Raghavachari, K., Foresman, J. B., Cioslowski, J., Ortiz, J. V., Stefanov, B. B., Liu, G., Liashenko, A., Piskorz, P., Gonzalez, C., Challacombe, M., Gill, P. M. W., Johnson, B. G., Chen, W., Wong, M. W., Andres, J. L., Head-Gordon, M., Replogle, E. S., and Pople, J. A. (1998) Gaussian 98, revision A.7, Gaussian Inc., Pittsburgh, PA.
68. Bayly, C. I., Cieplak, P., Cornell, W. D., and Kollman, P. A. (1993) A well-behaved electrostatic potential based method using charge restraints for determining atom-centered charges: The RESP model, *J. Phys. Chem. 97*, 10269−10280.
69. Cornell, W. D., Cieplak, P., Bayly, C. I., Gould, I. R., Merz, K. M., Jr., Ferguson, D. M., Spellmeyer, D. C., Fox, T., Caldwell, J. W., and Kollman, P. A. (1995) A second generation force field for the simulation of proteins, nucleic acids, and organic molecules, *J. Am. Chem. Soc. 117*, 5179−5197.
70. Wang, J., Wolf, R. M., Caldwell, J. W., Kollman, P. A., and Case, D. A. (2004) Development and testing of a general Amber force field, *J. Comput. Chem. 25*, 1157−1174.
71. Duan, Y., Wu, C., Chowdhury, S., Lee, M. C., Xiong, G., Zhang, W., Yang, R., Cieplak, P., Luo, R., and Lee, T. (2003) A point-charge force field for molecular mechanics simulations of proteins, *J. Comput. Chem. 24*, 1999−2012.
72. Jorgensen, W., Chandrasekhar, J., Mandura, J., Impey, R., and Klein, M. (1983) Comparison of simple potential functions for simulating liquid water, *J. Phys. Chem. 79*, 926−935.
73. Berendsen, H. J. C., Postma, J. P. M., van Gunsteren, W. F., DiNola, A., and Haak, J. R. (1984) Molecular dynamics with coupling to an external bath, *J. Chem. Phys. 81*, 3684−3690.
74. Ryckaert, J.-P., Ciccotti, G., and Berendsen, H. J. C. (1977) Numerical integration of the Cartesian equations of motion of a system with constraints: molecular dynamics of n-alkanes, *J. Comput. Phys. 23*, 327−341.
75. Darden, T., York, D., and Pedersen, L. (1993) Particle mesh Ewald−an Nlog(N) method for Ewald sums in large systems, *J. Chem. Phys. 98*, 10089−10092.
76. Wu, Y.-D., Lai, D. K. W., and Houk, K. N. (1995) Transition structures of hydride transfer reactions of protonated pyridinium ion with 1,4-dihydropyridine and protonated nicotinamide with 1,4-dihydronicotinamide, *J. Am. Chem. Soc. 117*, 4100−4108.
77. Delano, W. L. (2002) The PyMOL molecular graphics system, DeLano Scientific, San Carlos, CA.
78. Quirk, P. G., Smith, K. J., Thomas, C. M., and Jackson, J. B. (1999) The mobile loop region of the NAD(H)-binding component (dI) of proton-translocating transhydrogenase from *Rhodospirillum rubrum*: complete NMR assignment and effects of bound nucleotides, *Biochim. Biophys. Acta 1412*, 139−148.
79. Bizouarn, T., Diggle, C., and Jackson, J. B. (1996) The binding of nucleotides to domain I proteins of the proton-translocating transhydrogenases of *Rhodospirillum rubrum* and *Escherichia coli* as measured by equilibrium dialysis, *Eur. J. Biochem. 239*, 737−741.
80. Grimley, R. L., Quirk, P. G., Bizouarn, T., Thomas, C. M., and Jackson, J. B. (1997) The role of methionine-239, an amino acid residue in the mobile loop region of proton-translocating transhydrogenase, *Biochemistry 36*, 14762−14770.
81. Fjellstrom, O., Johansson, C., and Rydstrom, J. (1997) Structural and catalytic properties of the expressed and purified NAD(H)- and NADP(H)-binding domains of proton-pumping transhydrogenase from *Escherichia coli*, *Biochemistry 36*, 11331−11341.
82. Bergkvist, A., Johansson, C., Johansson, T., Rydstrom, J., and Karlsson, B. G. (2000) Interactions of the NADP(H)-binding

domain III of proton-translocating transhydrogenase from *Escherichia coli* with NADP(H) and the NAD(H)-binding domain I studied by NMR and site-directed mutagenesis, *Biochemistry 39*, 12595−12605.
83. Sundaresan, V., Yamaguchi, M., Chartron, J., and Stout, C. D. (2003) Conformational change in the NADP(H)-binding domain of transhydrogenase defines four states, *Biochemistry 42*, 12143−12153.
84. Bizouarn, T., Stilwell, S. N., Venning, J. M., Cotton, N. P. J., and Jackson, J. B. (1997) The pH dependences of reactions catalysed by the complete proton-translocating transhydrogenase from *Rhodospirillum rubrum*, and by the complex formed from its recombinant peripheral, nucleotide-binding domains, *Biochim. Biophys. Acta 1322*, 19−32.
85. Bizouarn, T., van Boxel, G. I., Bhakta, T., and Jackson, J. B. (2005) Nucleotide binding affinities of the intact proton-translocating transhydrogenase from *Escherichia coli*, *Biochim. Biophys. Acta 1708*, 404−410.
86. Brondijk, T. H. C., van Boxel, G. I., Singh, A., Mather, O. M., White, H. A., Quirk, P. G., White, S. A., and Jackson, J. B. (2006) The role of invariant amino acid residues at the hydride-transfer site of proton-translocating transhydrogenase, *J. Biol. Chem. 281*, 13345−13354.
87. van Boxel, G. I., Quirk, P., Cotton, N. J. P., White, S. A., and Jackson, J. B. (2003) Glutamine-132 in the NAD(H)-binding component of proton-translocating transhydrogenase tethers the nucleotides before hydride transfer, *Biochemistry 42*, 1217−1226.
88. Pinheiro, T. J. T., Venning, J. D., and Jackson, J. B. (2001) Fast hydride transfer in proton-translocating transhydrogenase revealed in a rapid-mixing, continuous-flow device, *J. Biol. Chem. 276*, 44757−44761.
89. Singh, A., Venning, J. D., Quirk, P., van Boxel, G. I., Rodrigues, D. J., White, S. A., and Jackson, J. B. (2003) Interactions between transhydrogenase and thio-nicotinamide analogues of NAD(H) and NADP(H) underline the importance of nucleotide conformational changes in coupling to proton translocation, *J. Biol. Chem. 278*, 33208−33216.
90. Johansson, C., Pedersen, A., Karlsson, B. G., and Rydstrom, J. (2002) Redox-sensitive loops D and E regulate NADP(H) binding in domain III and domain I-domain III interactions in proton-translocating *Escherichia coli* transhydrogenase, *Eur. J. Biochem. 269*, 4505−4515.
91. Yu, Y., and Samuelson, J. (1994) Primary structure of an *Entamoeba histolytica* nicotinamide nucleotide transhydrogenase, *Mol. Biochem. Parasitol. 68*, 323−328.
92. Clark, C. G., and Roger, A. J. (1995) Direct evidence for secondary loss of mitochondria in *Entamoeba histolytica*, *Proc. Natl. Acad. Sci. U.S.A. 92*, 6518−6521.
93. Kramer, R. A., Tomchak, L. A., McAndrew, S. J., Becker, K., Hug, D., Pasamontes, L., and Humbelin, M. (1993) An *Eimeria tenella* gene encoding a protein with homology to the nucleotide transhydrogenase of *Escherichia coli* and bovine mitochondria, *Mol. Biochem. Parasitol. 60*, 327−332.
94. Vermeulen, A. N., Kok, J. J., Van Den Boogart, P., Dijkema, R., and Claessens, J. A. J. (1993) Eimeria refractile body proteins contain two potential functional charcteristics: Transhydrogenase and carbohydrate transport, *FEMS Micobiol. Lett. 110*, 223−230.
95. Weston, C. J., Venning, J. D., and Jackson, J. B. (2002) The membrane-peripheral subunits of transhydrogenase from *Entamoeba histolytica* are functional only when dimerized, *J. Biol. Chem. 277*, 26163−26170.
96. Weston, C. J., White, S. A., and Jackson, J. B. (2001) The unusual transhydrogenase of *Entamoeba histolytica*, *FEBS Lett. 488*, 51−54.

BI061843R